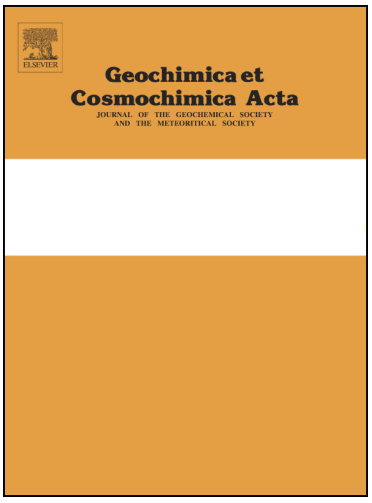

The isotope effect of nitrate assimilation in the Antarctic Zone: Improved estimates and paleoceanographic implications

François Fripiat, Alfredo Martínez-García, Sarah E. Fawcett, Preston C. Kemeny, Anja S. Studer, Sandi M. Smart, Florian Rubach, Sergey Oleynik, Daniel M. Sigman, Gerald H. Haug

PII: S0016-7037(18)30682-3
DOI: https://doi.org/10.1016/j.gca.2018.12.003
Reference: GCA 11036

To appear in: *Geochimica et Cosmochimica Acta*

Received Date: 11 June 2018
Revised Date: 28 November 2018
Accepted Date: 5 December 2018

Please cite this article as: Fripiat, F., Martínez-García, A., Fawcett, S.E., Kemeny, P.C., Studer, A.S., Smart, S.M., Rubach, F., Oleynik, S., Sigman, D.M., Haug, G.H., The isotope effect of nitrate assimilation in the Antarctic Zone: Improved estimates and paleoceanographic implications, *Geochimica et Cosmochimica Acta* (2018), doi: https://doi.org/10.1016/j.gca.2018.12.003

The isotope effect of nitrate assimilation in the Antarctic Zone: Improved estimates and paleoceanographic implications

François Fripiat[1], Alfredo Martínez-García[1], Sarah E. Fawcett[2], Preston C. Kemeny[3,4], Anja S. Studer[1], Sandi M. Smart[5], Florian Rubach[1], Sergey Oleynik[4], Daniel M. Sigman[4] and Gerald H. Haug[1]

[1]Max Planck Institute for Chemistry, Mainz, Germany

Corresponding author: f.fripiat@mpic.de

[2]Department of Oceanography, University of Cape Town, Rondebosch, South Africa

[3]Division of Geological and Planetary Sciences, California Institute of Technology, Pasadena, California, USA

[4]Department of Geosciences, Princeton University, Princeton, New Jersey, USA

[5]Department of Earth Sciences, Stellenbosch University, Matieland, Stellenbosch, South Africa

Abstract

Both the nitrogen (N) isotopic composition ($\delta^{15}N$) of the nitrate source and the magnitude of isotope discrimination associated with nitrate assimilation are required to estimate the degree of past nitrate consumption from the $\delta^{15}N$ of organic matter in Southern Ocean sediments (e.g., preserved within diatom microfossils). It has been suggested that the amplitude of isotope discrimination (i.e. the isotope effect) correlates with mixed layer depth, driven by a physiological response of phytoplankton to light availability, which introduces complexity to the interpretation of sedimentary records. However, most of the isotope effect estimates that underpin this hypothesis derive from acid-preserved water samples, from which nitrite would have been volatilized and lost during storage. Nitrite $\delta^{15}N$ in Antarctic Zone surface waters is extremely low (-61 ± 20‰), consistent with the expression of an equilibrium isotope effect associated with nitrate–nitrite interconversion. Its loss from the combined nitrate+nitrite pool would act to raise the $\delta^{15}N$ of nitrate, potentially yielding overestimation of the isotope effect. Here, we revisit the nitrate assimilation isotope effect in the Antarctic Zone with measurements of the $\delta^{15}N$ and concentration of nitrate with and without nitrite, using frozen sea water samples from 5 different cruises that collectively cover all sectors of the Southern Ocean. The N isotope effect estimated using nitrate+nitrite $\delta^{15}N$ is relatively constant (5.5 ± 0.6‰) across the Antarctic Zone, shows no relationship with mixed layer depth, and is in agreement with sediment trap $\delta^{15}N$ measurements. Estimates of the N isotope effect derived from nitrate-only $\delta^{15}N$ are higher and more variable (7.9 ± 1.5‰), consistent with an artifact from nitrate-nitrite isotope exchange. In the case of the Southern Ocean, we conclude that the $\delta^{15}N$ of nitrate+nitrite better reflects the isotope effect of nitrate

assimilation. The stability of this isotope effect across the Antarctic Zone simplifies the effort to reconstruct past degree of nitrate consumption.

1. Introduction

In the Southern Ocean and especially south of the Polar Front (i.e. the Antarctic Zone), deep nutrient-rich waters rise to the surface and are returned to the subsurface before nitrate and phosphate are fully used by phytoplankton. The ineffectiveness of phytoplankton at drawing down major nutrients in Southern Ocean surface waters has been attributed to co-limitation by iron and light (Martin et al., 1990; Mitchell et al., 1991) and allows (i) CO_2 sequestered in the deep ocean to be released to the atmosphere (Sigman et al., 2010) and (ii) the unused nutrient pool in the surface waters of the Southern Ocean to be exported to the low latitudes (Sarmiento et al., 2004; Palter et al., 2010).

Nitrate (NO_3^-) assimilation by phytoplankton preferentially incorporates ^{14}N into new biomass, leaving the residual NO_3^- pool enriched in ^{15}N (Wada and Hattori, 1978; Montoya and McCarthy, 1995; Granger et al., 2004, 2010). The kinetic isotope effect (ε) expresses the degree of isotope discrimination, and is commonly defined as the ratio of reaction rates at which the two isotopes are converted from reactant to product (i.e. $\varepsilon\ (‰) = ((1- {}^{15}k/{}^{14}k) \times 1000)$; where ${}^{x}k$ is the rate constant for the ^{x}N-containing reactant). The isotopic fractionation of NO_3^- assimilation links the degree of NO_3^- consumption to the $\delta^{15}N$ (= $(({}^{15}N/{}^{14}N)_{sample}/({}^{15}N/{}^{14}N)_{reference}-1)x1000$, with atmospheric N_2 as the reference) of both the NO_3^- and the newly produced organic matter (Altabet and François, 1994; Sigman et al., 1999a). Thus, the $\delta^{15}N$ of fossil-bound organic matter recovered from Southern Ocean sediment cores provides a measure of the degree of nitrate consumption in the past and has been used to investigate possible mechanisms for driving the changes in atmospheric CO_2 observed over glacial cycles (Robinson and Sigman, 2008; Martinez-Garcia et al., 2014; Studer et al., 2015; Wang et al., 2017).

During at least the last two ice ages, the $\delta^{15}N$ of diatom- and deep-sea coral-bound organic N in Antarctic sediments was ~4‰ higher than it is today (Studer et al., 2015; Wang et al., 2017), indicative of an enhanced degree of nitrate consumption during the ice ages. Together with the observed glacial decrease in Antarctic productivity (Kohfeld et al., 2005; Jaccard et al., 2013), this implies that the supply of NO_3^- to Antarctic Zone surface waters was significantly reduced during the ice ages, leading to the hypothesis of Antarctic "stratification" as one of the dominant drivers of glacial-interglacial variation in atmospheric pCO_2 (Francois et al., 1997; Sigman et al., 2010).

The $\delta^{15}N$ of the NO_3^- supply and the isotope effect of NO_3^- assimilation are two key parameters required for estimating the degree of past NO_3^- consumption. Previous studies in the Southern Ocean

have suggested systematic variations in the isotope effect with mixed layer depth that would have implications for the $\delta^{15}N$ of sinking particulate N (PN) and fossil-bound N under changing environmental conditions (DiFiore et al., 2010). However, most of these measurements were made on acidified water samples, from which nitrite (NO_2^-) would have been largely lost during storage, due to the volatility of HNO_2 followed by its rapid conversion into gaseous nitrogen oxide (NO and NO_2) (Park and Lee, 1988; Rayson et al., 2012). NO_2^- can be reliably removed prior to isotope analysis through the addition of sulfamic acid or sulfanilamide, allowing the measurement of both NO_3^-+NO_2^- and NO_3^--only $\delta^{15}N$ and $\delta^{18}O$ for seawater samples stored frozen since collection (Granger and Sigman, 2009; Weigand et al., 2016). In late-summer water column profiles, Kemeny et al. (2016) reported a systematic difference between NO_3^-+NO_2^- $\delta^{15}N$ and NO_3^- $\delta^{15}N$ in Antarctic Zone surface waters, with NO_3^- $\delta^{15}N$ typically being 0.5-1.0‰ higher than NO_3^-+NO_2^- $\delta^{15}N$. They suggested that NO_3^--NO_2^- interconversion occurs in the euphotic zone, leading to the expression of an N equilibrium isotope effect between NO_3^- and NO_2^-, enriching NO_3^- and depleting NO_2^- in ^{15}N. Seasonal mixed layer deepening was suggested to entrain nitrite oxidizers from the subsurface into the late-summer mixed layer, discouraging NO_2^- oxidation due to light inhibition and favoring the reversibility of the nitrite oxidoreductase (NXR) enzyme.

In this study, we revisit the mean value and variability of the isotope effect of NO_3^- assimilation in the Antarctic Zone using isotopic data from seawater samples that were stored frozen and not acidified, thus avoiding potential artifacts from the coupling of putative NO_3^--NO_2^- interconversion with subsequent NO_2^- loss during storage.

2. Materials and methods:

2.1. Background: hydrography

We draw a distinction between the Polar Antarctic Zone (PAZ), the area south of the Southern Antarctic Circumpolar Current Front (SACFF), and the Open Antarctic Zone (OAZ), the area between the SACCF and the Polar Front (Fig. 1) (e.g., Sigman et al., 2009a). The boundary between these two zones is also roughly delineated by either the northernmost extent of winter sea-ice or the southernmost extent of Upper Circumpolar Deep Water (UCDW) (Orsi et al., 1995).

Across the Antarctic Zone, NO_3^- is supplied by Ekman pumping and vertical mixing across the base of the winter mixed layer. Nutrient-rich Circumpolar Deep Water (CDW) upwells in the Antarctic Zone. Part of the upwelled CDW gains buoyancy due to warming and freshening, causing it to flow northward in the Ekman layer, ultimately sinking north of the Polar Front into the main oceanic pycnocline. The remainder loses buoyancy near Antarctica, inducing deep convection over the continental shelves and

leading to Antarctic Bottom Water (AABW) formation (Fig. 2). Deep ventilation may also occur in the Antarctic Zone away from the coasts, for example, due to mixing by mesoscale eddies (Abernathey and Ferreira, 2015).

In summer, the upper halocline layer in most of the Antarctic Zone (hereafter referred as Antarctic Surface Water, AASW) is characterized by both a relatively fresh, well-mixed surface layer, and a subsurface temperature minimum (T_{min}) layer below (Figs. 2c and A1c; hereafter referred to as the 'T_{min}' stations) (e.g., Park et al., 1998). The latter is also known as "Winter Water" because it is the remnant of the previous winter mixed layer that has become isolated in the shallow subsurface by spring-to-summer warming and freshening of the overlying water. AASW tends to be thicker in the OAZ due to higher wind stress and thus deeper vertical mixing near the Polar Front, with generally shallower mixed layers in the seasonally sea-ice covered areas to the south (Fig. 1) (Pellichero et al., 2017). Near and above the continental shelves (hereafter referred as to the 'margin' stations), a shallow mixed layer usually caps a relatively homogeneous, dense, near-freezing shelf water mass. The latter has undergone a brine rejection-driven increase in salinity, a prerequisite for the formation of AABW (e.g., Orsi et al., 1999). As a result of lateral exchange, intrusion of AASW and CDW southward toward the continental shelves can generate a distinct subsurface temperature maximum between the summertime mixed layer and the shelf waters below (hereafter referred to as the 'T_{max}' stations) (e.g., DiFiore et al., 2009).

2.2. Sample collection

New and previously published NO_3^-+NO_2^- and NO_3^--only $\delta^{15}N$ and $\delta^{18}O$ measurements are reported from the Atlantic, Indian, and Pacific sectors of the Antarctic Zone (Fig. 1 and Table 1). New hydrographic sections are GOSHIP IO8S (February 2016) in the eastern Indian sector, P18S (January 2017) in the eastern Pacific sector, and SANAE54 (December-January 2014-2015) in the Atlantic sector along the Greenwich Meridian. These new datasets are compiled in combination with previous measurements located near the Antarctic continent (DiFiore et al. 2009; NBP cruises) and in the western Pacific sector (Kemeny et al. 2016; GOSHIP P16S transect).

A total of 50 hydrocasts (24 unpublished) were collected between the Antarctic continental shelf and the Polar Front. Most of the hydrocasts (n = 46) were collected between December 12th and April 9th during the various years (Table 1). This summer-early fall condition captures the major extent of annual NO_3^- depletion in the mixed layer. Four hydrocasts from the Ross Sea (NBP01-01) were sampled in November at the onset of the growing period (DiFiore et al., 2009). Unfiltered water samples were collected and immediately frozen (-20°C) until their analysis at home-based laboratories (Max Planck Institute for Chemistry (MPIC) for IO8S and P18S and Princeton University for SANAE54).

2.3. Nitrate isotope analysis

NO_3^-+NO_2^- $\delta^{15}N$ and $\delta^{18}O$ were determined using the denitrifier method (Sigman et al., 2001; Casciotti et al., 2002; Weigand et al., 2016). Briefly, 10-20 nmol of NO_3^-+NO_2^- was quantitatively converted to N_2O gas by a strain of denitrifying bacteria (*Pseudomonas chlororaphis f. sp. aureofaciens* ATCC n°13985) that lacks an active N_2O reductase enzyme. In both laboratories, the isotopic composition of N_2O was measured by gas chromatography/isotope ratio mass spectrometry using a purpose-built online N_2O extraction and purification system and Thermo MAT 253 mass spectrometer (Weigand et al., 2016). Measurements are referenced to air N_2 for $\delta^{15}N$ and Vienna Standard Mean Ocean Water (VSMOW) for $\delta^{18}O$ using the NO_3^- reference materials IAEA-NO3, with a $\delta^{15}N$ of 4.7‰ and a $\delta^{18}O$ of 25.6‰, and USGS-34, with a $\delta^{15}N$ of -1.8‰ and a $\delta^{18}O$ of -27.9‰ (Böhlke et al., 2003).

During the reduction of NO_3^- and NO_2^- to N_2O by the denitrifier method, O atoms are either transferred to the resulting nitrogen oxide pool (ultimately to N_2O) or lost as water, and isotopic fractionation is known to occur during these branching reactions (Casciotti et al., 2002). For NO_3^-, this effect is accounted for by calibration with NO_3^- isotopic reference materials. Because NO_2^- reduction to N_2O represents a smaller fractional loss of oxygen atoms than NO_3^- reduction (3/4 vs. 5/6), the N_2O generated from NO_2^- by the denitrifier method is ~25‰ lower in $\delta^{18}O$ than N_2O generated from NO_3^- with the same initial $\delta^{18}O$ (Casciotti et al., 2007). This methological bias is corrected for each sample by adding to NO_3^-+NO_2^- $\delta^{18}O$ the product of 25‰ and the relative contribution of NO_2^- to NO_3^-+NO_2^- (Kemeny et al., 2016). In order to isolate and measure the NO_3^--only $\delta^{15}N$ and $\delta^{18}O$, samples with detectable NO_2^- concentrations were treated with sulfamic acid prior to NO_3^- isotope analysis (Granger and Sigman, 2009).

Replicate analyses (100% of the samples) at MPIC indicate median 1sd reproducibility of <0.07‰ and <0.13‰ for $\delta^{15}N$ and $\delta^{18}O$, respectively (i.e., similar to <0.05‰ and <0.14‰ for P16S and SANAE54 analyzed at Princeton). There was no significant difference in reproducibility between samples treated with sulfamic acid and their untreated counterparts. Seawater samples from the deep North Atlantic (MPIC) and Pacific (Princeton University) were used as in-house standards and measured two to three times in each run, the long-term reproducibility was <0.08‰ and <0.12‰ for $\delta^{15}N$ and $\delta^{18}O$, respectively. In the case of the NBP samples, which were analyzed a decade earlier using the protocol and extraction system of Casciotti et al. (2002), the replicate analyses indicated a median 1sd reproducibility of 0.17‰ for $\delta^{15}N$ and 0.26‰ for $\delta^{18}O$ (DiFiore et al., 2009).

2.4. Estimating the isotope effect of nitrate assimilation

If NO_3^- assimilation proceeds with a constant isotope effect and if the reactant N pool (NO_3^-) is neither significantly replenished nor subject to any loss, then the isotopic evolution of the residual NO_3^-, instantaneous PN (hereafter indicated with the superscript "inst"), and accumulated PN (hereafter indicated with the superscript "acc") are described by Rayleigh fractionation kinetics, with the following equations (Mariotti et al., 1981):

$$R_{NO_3^-} = R^0_{NO_3^-}.f^{-\left(10^{-3}.\varepsilon\right)} \quad (1)$$

$$R^{inst}_{PN} = (1-10^{-3}.\varepsilon).R_{NO_3^-} \quad (2)$$

$$R^{acc}_{PN} = R^0_{NO_3^-}.\frac{1-f^{\left(1-10^{-3}.\varepsilon\right)}}{1-f} \quad (3)$$

where f is the fraction of NO_3^- remaining (i.e. f = $[NO_3^-]/[NO_3^-]_{initial}$), the superscript 0 is the initial condition, R is the $^{15}N/^{14}N$ or $^{18}O/^{16}O$ ratio, and ε is the isotope effect for either N or O isotopes. Since O atoms are not incorporated into biomass, only equation 1 is valid for the O isotopes. Because phytoplankton discriminate against ^{15}N and ^{18}O to the same extent during NO_3^- assimilation ($^{15}\varepsilon \approx {}^{18}\varepsilon$; Granger et al., 2004, 2010; Karsh et al., 2012, 2014), the residual NO_3^- $\delta^{15}N$ and $\delta^{18}O$ rise equally if only assimilation is taking place in a water parcel. Equations 1-3 include the reasonable assumption that the abundances of both the ^{15}N and ^{18}O isotope are low, implying that $^{14}N \sim {}^{14}N+{}^{15}N$ and $^{16}O \sim {}^{16}O+{}^{17}O+{}^{18}O$ (Mariotti et al., 1981). Rearranging equation (1) and using delta notation instead of the ratio allows us to formulate a linear relationship that has negative ε as its slope and initial conditions (NO_3^- concentration and $\delta^{15}N$) as intercept (Mariotti et al., 1981), as shown here for the N isotopes:

$$10^3.ln\left(10^{-3}.\delta^{15}N_{NO_3^-}+1\right) = -\varepsilon.ln([NO_3^-]) + \left(10^3.ln\left(10^{-3}.\delta^{15}N^0_{NO_3^-}+1\right) + \varepsilon.ln([NO_3^-]_0)\right) \quad (4)$$

In logarithmic equations of the form ln[(1+u)/(1+v)], where u and v are real numbers that are small relative to 1, which is the case for most $10^{-3}\cdot\delta$ values, ln[(1+u)/(1+v)] can be approximated by u – v. Consequently, equation (4) can be simplified to give the following widely applied approximate equation (Mariotti et al., 1981):

$$\delta^{15}N_{NO_3^-} = -\varepsilon.ln([NO_3^-]) + \left(\delta^{15}N^0_{NO_3^-} + \varepsilon.ln([NO_3^-]_0)\right) \quad (5)$$

We calculate a difference of less than ~0.1‰ between equations (4) and (5) for estimates of the NO_3^- assimilation isotope effect in the Antarctic Zone. While equation 5 is useful for illustrating Rayleigh fractionation trends in the plotting spaces of NO_3^- $\delta^{15}N$ *vs.* ln($[NO_3^-]$) and NO_3^- $\delta^{18}O$ *vs.* ln($[NO_3^-]$), we use the more accurate equation (4) to estimate isotope effects.

3. Results

3.1. Nitrite concentration and impact on isotope distribution

In all the Southern Ocean stations analyzed, there is a small but significant accumulation of NO_2^- near the surface, increasing from near-zero concentrations in deep water to ~ 0.25 μmol l^{-1} (Fig. 3). This is in contrast to low-latitude areas, where a primary NO_2^- maximum is typically found at the base of the euphotic layer, with <0.02 μmol l^{-1} in the surface mixed layer (Lomas and Lipschultz, 2006; Fawcett et al., 2015; Peng et al., 2018), but consistent with a recent compilation of observations for the high latitude ocean showing similarly elevated levels of NO_2^- throughout the mixed layer (Zakem et al., 2018). The removal of NO_2^- from samples with detectable NO_2^- concentrations has a significant impact on the nitrate isotope distribution (Figs. 4 and 5a). NO_3^--only $\delta^{15}N$ is higher than NO_3^-+NO_2^- $\delta^{15}N$ by ~0.7 ± 0.2‰ in the summer surface mixed layer, but it is not significantly different deeper in the water column. In contrast, there is no clear difference (0.0 ± 0.2‰) between NO_3^--only and NO_3^-+NO_2^- $\delta^{18}O$ throughout the upper water column (Figs. 4 and 5b).

3.2. Nitrate isotope distribution in the Antarctic Zone

The $\delta^{15}N$ and $\delta^{18}O$ of both NO_3^--only and NO_3^-+NO_2^- increase toward the surface in concert with the upward decline in NO_3^- concentration, reflecting the preferential assimilation of ^{14}N- and ^{16}O-bearing NO_3^- by phytoplankton (Figs 2 and 4). In the OAZ, NO_3^-+NO_2^- $\delta^{15}N$ increases from 5.0‰ in the deeper layers to 6.6‰ at the surface on average, and from 5.0‰ to 7.4‰ for NO_3^--only $\delta^{15}N$. Both NO_3^--only and NO_3^-+NO_2^- $\delta^{18}O$ increase to the same extent across this depth interval, from 1.9‰ to 3.7‰ on average. At the T_{min} stations in the PAZ, NO_3^-+NO_2^- $\delta^{15}N$ increases from 4.8‰ to 6.2‰ on average, and from 4.8‰ to 6.9‰ for NO_3^--only $\delta^{15}N$. Similar to the OAZ, both NO_3^--only and NO_3^-+NO_2^- $\delta^{18}O$ increase to the same extent, from 2.0‰ to 3.4‰. The northward increases in NO_3^--only and NO_3^-+NO_2^- $\delta^{15}N$ and $\delta^{18}O$ result from progressive NO_3^- consumption during the Ekman transport of surface water from the Antarctic Zone to the Polar Frontal and Subantarctic Zones (Figs. 2 and A1) (Sigman et al., 1999a; DiFiore et al., 2006).

Deep convection over the shelves mixes lower [NO_3^-] and higher $\delta^{15}N$ and $\delta^{18}O$ surface waters down into the ocean interior, causing these dense shelf waters to be depleted in NO_3^- concentration and elevated in the $\delta^{15}N$ and $\delta^{18}O$ of NO_3^-+NO_2^- and NO_3^--only relative to deep waters further north (Figs 2 and 4). Because of the lower degree of NO_3^- consumption at the PAZ margin stations, the increase in NO_3^--only and NO_3^-+NO_2^- $\delta^{15}N$ and $\delta^{18}O$ toward the surface is small and close to the analytical precision. At the PAZ T_{max} stations, a larger scatter is observed toward the surface but with similar mean properties

as for the PAZ T_{min} stations (Fig. 4). For these stations, the $\delta^{15}N$ or $\delta^{18}O$ of NO_3^--only were not measured (DiFiore et al., 2009).

4. Discussion

4.1. Nitrate supply to Antarctic surface waters

Below AASW lie two distinct water masses and, therefore, two different sources of NO_3^- to Antarctic Zone surface waters: Lower Circumpolar Deep Water (LCDW) and Upper Circumpolar Deep Water (UCDW), which supply NO_3^- to the PAZ and OAZ, respectively. UCDW is characterized on average by higher NO_3^- concentration and $\delta^{15}N$ than LCDW (by 1.5 µmol l^{-1} and 0.2-0.3‰, respectively; Sigman et al., 2000; DiFiore et al., 2010) but is similar in NO_3^- $\delta^{18}O$ (Figs. 2, 4, and A1).

The NO_3^- concentration maximum in UCDW results from exchange with the Indian and Pacific Oceans, where regenerated nutrients accumulate along the mid-depth return flow of the ocean's "conveyor belt" circulation (Sarmiento et al., 2007; Talley, 2013). The ^{15}N enrichment in UCDW ultimately derives from the transfer (via Ekman transport) of ^{15}N- and ^{18}O-enriched residual NO_3^- from the polar ocean to lower latitude intermediate, thermocline, and surface waters (Fig. 2; Sigman et al., 1999a; Rafter et al., 2013). In low-latitude areas where NO_3^- consumption is complete, export production and remineralization produce regenerated NO_3^- with the same $\delta^{15}N$ as the NO_3^- originally supplied to the euphotic zone from the underlying thermocline. The NO_3^- in the thermocline was, in turn, elevated in $\delta^{15}N$ (and $\delta^{18}O$) by partial NO_3^- consumption when the thermocline water was previously at the surface of the Antarctic zone (AZ), polar front zone (PFZ) and subantarctic zone (SAZ). Its regeneration thus elevates the $\delta^{15}N$ of UCDW and its deep Pacific and Indian precursors (e.g., Pacific Deep Water). The same processes do not elevate the NO_3^- $\delta^{18}O$ of UCDW because regenerated NO_3^- has a $\delta^{18}O$ equal to that of ambient water plus ~1.1‰ (Sigman et al., 2009a; Buchwald et al., 2012), which is lower than the ambient NO_3^- $\delta^{18}O$ (> 1.8‰). Water column denitrification in the tropical oxygen deficient zones also works to increase the NO_3^- $\delta^{15}N$ in this mid-depth return flow, again causing a much weaker increase in NO_3^- $\delta^{18}O$ due to the low latitude NO_3^- assimilation/regeneration cycle described above (Sigman et al., 2009b).

4.2. Nitrate isotope variation in Antarctic surface waters

4.2.1. Nitrite interference and the interconversion of nitrate and nitrite

During the analysis of the NO_3^- isotopes by N_2O-based methods, both NO_3^- and NO_2^- are converted to N_2O, but the contribution from NO_2^- to the measured isotopic composition is often considered negligible

due to its typically low concentration relative to NO_3^- in seawater (Sigman et al., 2001; Casciotti et al., 2002; McIlvin and Altabet, 2005). However, in the Southern Ocean mixed layer, there is commonly a small but significant accumulation of NO_2^- near the surface. Most of the previous NO_3^- isotope measurements in the Southern Ocean have been performed on acidified samples (Sigman et al., 1999a; Altabet and François, 2001; Karsh et al., 2003; DiFiore et al., 2006), which would have affected the preservation of NO_2^-. Under acidic conditions, nitrous acid (HNO_2) forms, some of which may be lost to the gas phase. In addition, HNO_2 can decompose to nitrogen oxides (NO and NO_2), with some of the NO_2 being hydrolyzed to form NO_3^- and the rest escaping from the high-density polyethylene sample bottles typically used for storage (Park and Lee, 1988; Rayson et al., 2012). NO_2^- disappearance during storage could plausibly be argued to be beneficial for the understanding of the isotope dynamics associated with NO_3^- assimilation, with the caveat that a portion of the HNO_2 breakdown can yield NO_3^-. Freezing of seawater samples is thought to better preserve both NO_3^- and NO_2^- concentrations as well as their $\delta^{15}N$ and $\delta^{18}O$ values, a view that is supported by the stability of $\delta^{15}N$ and $\delta^{18}O$ of NO_3^-+NO_2^- measurements in frozen samples over time (e.g., Smart et al., 2015; Kemeny et al., 2016; this study).

Because of the small NO_2^- contribution to the NO_3^-+NO_2^- pool (<1%) in the Southern Ocean, prior studies assumed NO_2^- to have a negligible effect on NO_3^-+NO_2^- $\delta^{15}N$ and $\delta^{18}O$ (DiFiore et al., 2009). However, applying NO_2^- removal to Southern Ocean surface mixed layer samples has shown that NO_2^- can have a significant effect on NO_3^-+NO_2^- $\delta^{15}N$, challenging those previous assumptions (Rafter et al., 2013; Smart et al., 2015; Kemeny et al., 2016). This is further confirmed by our compilation, in which NO_3^--only $\delta^{15}N$ is higher than NO_3^-+NO_2^- $\delta^{15}N$ by ~0.7 $\pm$ 0.2‰ in the summer surface mixed layer but is not significantly different deeper in the water column (Fig. 5a). Given the small contribution of NO_2^- to the NO_3^-+NO_2^- pool (median = 0.9%), the $\delta^{15}N$ difference implies that NO_2^- $\delta^{15}N$ is extremely low, ranging from -90‰ to -17‰ (averaging -61 $\pm$ 20‰) in the mixed layer and increasing with depth toward ~ 0‰ at the T_{min} (Fig. 3).

NO_2^- is thought to be generated in the subsurface largely as a result of the low-light conditions. Here, NO_2^- is produced during the first step of nitrification ($NH_4^+ \rightarrow NO_2^-$) and as a result of efflux of NO_2^- out of phytoplankton cells due to an imbalance between NO_3^- and NO_2^- reduction during assimilatory NO_3^- uptake. NO_2^- is consumed by both the second step of nitrification ($NO_2^- \rightarrow NO_3^-$) and NO_2^- assimilation by phytoplankton (Ward, 1985; Lomas and Lipschultz, 2006). This combination of processes can yield NO_2^- with a $\delta^{15}N$ between ~ 0‰ and -35‰, depending on the isotope effects of each process and their relative contributions to NH_4^+ and NO_2^- removal (Fripiat et al., 2015a). We observe NO_2^- $\delta^{15}N$ values that

fall roughly within this range in the subsurface (i.e., below the mixed layer), consistent with NO_2^- being produced and consumed by the processes outlined above.

However, another mechanism is required to produce the extremely low NO_2^- $\delta^{15}N$ estimated for the surface mixed layer (Fig. 3) and thus explain the measured $\delta^{15}N$ difference between NO_3^-+NO_2^- and NO_3^- only (Fig. 5a). Kemeny et al. (2016; P16S, Fig. 1) suggested that NO_3^--NO_2^- interconversion can occur in the Southern Ocean mixed layer. This interconversion would lead to the expression of the large equilibrium N isotope effect between NO_3^- and NO_2^- (60-90‰ under relevant conditions) (Casciotti, 2009; Kemeny et al., 2016), enriching NO_3^- and depleting NO_2^- in ^{15}N and yielding NO_3^- and NO_2^- with $\delta^{15}N$ values in the ranges that we observe (Figs. 3 and 5a). At this time, the expression of the equilibrium isotope effect between NO_3^- and NO_2^- is the only viable proposal for generating the observed extreme depletions of NO_2^- $\delta^{15}N$.

Most of the stations in both the PAZ and OAZ are found to have low NO_2^- $\delta^{15}N$ in the mixed layer, suggesting that NO_3^--NO_2^- interconversion is ubiquitous in summer in these regions, and not only in fall as suggested by Kemeny et al. (2016). Deep mixed layers prevail in the Southern Ocean (down to ~100m in December), and mixed layer depth (MLD) commonly exhibits short-term variability of up to 40m during the summer months (Pellichero et al., 2017; Holte et al., 2017). Subsurface microbial communities (i.e., nitrifiers) may end up trapped in the mixed layer following their entrainment into it such that they spend a significant amount of time in the euphotic layer (Fripiat et al., 2015b). Once in the mixed layer with elevated levels of light, light-inhibition is likely to decrease the activity of NO_2^- oxidizers and, therefore, the unidirectional oxidation of NO_2^- to NO_3^- (Ward et al., 1985; Vanzella et al., 1989). Under these conditions and according to Kemeny et al. (2016), the bifunctional nitrite oxidoreductase enzyme may catalyze both the forward and reverse reactions, enriching NO_3^- and depleting NO_2^- in ^{15}N. The effective co-occurrence of NO_2^- oxidation and NO_3^- reduction in the same intracellular (or periplasmic) space could allow for the full expression of the equilibrium isotope effect at the environmental scale. While the biological catalysis of NO_3^--NO_2^- equilibrium has previously been demonstrated in culture studies (Sundermeyer-Klinger et al., 1984; Friedman et al., 1986; Brunner et al., 2013; Wunderlich et al., 2013), the existence and operation of specific microbial consortia and enzymatic machinery that could explain our observations remains speculative.

From the perspective of the N atoms in NO_3^-+NO_2^-, interconversion operates as a closed system, with N atoms exchanged between NO_3^- and NO_2^- without the NO_3^-+NO_2^- pool experiencing any N loss or gain. This means that $^{15}\varepsilon$ associated with the assimilation of NO_3^-+NO_2^- should be unaffected by NO_3^--NO_2^- interconversion. However, as interconversion enriches NO_3^- in ^{15}N, the NO_3^--only $^{15}\varepsilon$ will be affected, and

will be larger than the NO_3^-+NO_2^- $^{15}\varepsilon$ (Table 1; Figs. 6a and 6b). Consistent with Kemeny et al. (2016), we observe that the $^{15}\varepsilon$ derived from NO_3^--only profiles is higher than the $^{15}\varepsilon$ derived from profiles of NO_3^- +NO_2^- (Fig. 7a). However, in contrast to the observation of Kemeny et al. (2016), our larger dataset suggests that there is no relationship between MLD and the difference in $^{15}\varepsilon$ estimated from the NO_3^- +NO_2^- and NO_3^--only data (R^2 = 0.01; p-value = 0.63) (Fig. 7a). The $^{15}\varepsilon$ difference has been suggested to reflect the extent of mixed layer NO_3^--NO_2^- interconversion at any given location. However, we hypothesize that short-term variability in the MLD provides an efficient mechanism for entrainment of the subsurface microbial communities (i.e., nitrifiers) into the euphotic layer, largely independent of the seasonal average MLD. This is likely to lead to conditions favorable for NO_3^--NO_2^- interconversion. Moreover, the mean (± 1sd) $^{15}\varepsilon$ difference (for NO_3^-+NO_2^- versus NO_3^-) is similar for stations in the OAZ (2.9 ± 1.3‰) and the PAZ (2.8 ± 1.9‰). In the PAZ, sea-ice melting in spring-summer seeds the mixed layer with a sea-ice microbial community, which grew in a low-light environment that is favorable to nitrification (Priscu et al., 1990; Fripiat et al., 2014), and the nitrifiers of this community may also facilitate NO_3^--NO_2^- interconversion in the mixed layer.

From the perspective of the O atoms in NO_3^-+NO_2^-, nitrate-nitrite interconversion implies an open system in which both the NO_3^--only and NO_3^-+NO_2^- pools are continuously supplied with O deriving predominantly from water (Kemeny et al., 2016). This is illustrated by comparing $^{15}\varepsilon$ with $^{18}\varepsilon$ for either NO_3^--only or NO_3^-+NO_2^-. The estimates of $^{18}\varepsilon$ tend to fall below the 1:1 relationship with $^{15}\varepsilon$ expected from NO_3^- assimilation alone (Fig. 8; Granger et al., 2004, 2010; Karsh et al., 2012). This can be explained by the incorporation of low-$\delta^{18}O$ O atoms from ambient H_2O into either NO_2^- or NO_3^- during NO_3^--NO_2^- interconversion (Kemeny et al., 2016). This process would propagate the low-$\delta^{18}O$ anomaly into both the NO_3^-+NO_2^- and NO_3^--only $^{18}\varepsilon$, consistent with the similar values of $^{18}\varepsilon$ that we estimate from the NO_3^- +NO_2^- and NO_3^--only data (Table 1; Figs. 6c and 6d). However, the very low concentration ratios of NO_2^- to NO_3^- may mask a large range in NO_2^- $\delta^{18}O$ (~50‰) that yield no significant difference (± 0.2‰) in NO_3^- +NO_2^- and NO_3^--only $\delta^{18}O$, precluding an assessment of the O isotope systematics of NO_3^--NO_2^- interconversion. We expect kinetic isotope effects during the incorporation and removal of O atoms, as well as equilibrium isotope effects between both NO_3^- and NO_2^- and NO_3^-+NO_2^- and water (e.g., Buchwald et al., 2012).

We conclude that, in the AZ, the N isotopic composition of NO_3^-+NO_2^- is more representative than that of NO_3^--only with regard to the true isotope effect of NO_3^- assimilation because NO_3^--only $^{15}\varepsilon$ is altered during the putative NO_3^--NO_2^- interconversion due to ^{15}N-enrichment. The $^{18}\varepsilon$ estimated from both NO_3^-

+NO_2^- and NO_3^--only is also vulnerable to alteration during interconversion, with O atoms likely being exchanged with water and then redistributed between NO_3^- and NO_2^- in the process.

4.2.2. Isotope fractionation during nitrate assimilation in Antarctic Surface Waters

The negative correlation between [NO_3^-] and both NO_3^- $\delta^{15}N$ and $\delta^{18}O$ reflects the link between NO_3^- consumption and the NO_3^- isotopes in the Antarctic Zone (Fig. 6), whereby preferential assimilation of ^{14}N and ^{16}O by phytoplankton leaves the residual NO_3^- pool enriched in ^{15}N and ^{18}O (Sigman et al., 1999a). There is strong seasonality associated with both the supply of NO_3^- to the mixed layer and consumption by phytoplankton. Primary production and NO_3^- assimilation are restricted to the late spring and summer when total insolation is higher and surface mixed layers are shallower. Nitrate supply to the water column above the base of the winter mixed layer occurs year-round, but nitrate supply to the sunlit surface waters is dominated by wintertime vertical mixing. A high ratio of assimilation to supply is therefore expected during the productive period, and the isotope fractionation associated with nutrient consumption is likely to approximate Rayleigh fractionation kinetics (Eqs. 1 to 5, section 2.3) (DiFiore et al., 2010; Fripiat et al., 2012). Accordingly, NO_3^- assimilation in AASW should generate a linear trend in NO_3^- $\delta^{15}N$ *vs*. ln([NO_3^-]) and $\delta^{18}O$ vs. ln([NO_3^-]) space starting from LCDW and UCDW values in the PAZ and OAZ, respectively (blue and red dashed lines in Fig. 6).

The data generally fall on a single $\delta^{18}O$/(ln[NO_3^-]) line consistent with a Rayleigh trend connecting deep water below AASW with the summertime mixed layer (Figs. 6c and 6d). In both the PAZ and OAZ, there is a similar progressive ^{18}O enrichment (~ 0.2‰) in the mean profiles from the deeper layers up to below AASW, despite the lack of a clear decline in NO_3^- concentration. This small ^{18}O enrichment may be caused by the co-occurrence of partial assimilation and subsurface nitrification (Fawcett et al., 2015; Peng et al., 2018), which will cause the $\delta^{18}O$ of NO_3^- in the upper ocean to increase upwards because the assimilated NO_3^- is initially lower in $\delta^{18}O$ (~ -3‰ to -2‰) than the regenerated NO_3^- produced by nitrification (i.e., ~ H_2O $\delta^{18}O$ + 1.1‰; Sigman et al., 2009).

The AASW NO_3^- $\delta^{15}N$/(ln[NO_3^-]) relationship displays upward concavity that causes T_{min} samples to fall below a Rayleigh fractionation trend with CDW as the NO_3^- source, by 0.2‰ and 0.5‰ for the PAZ and OAZ, respectively (Figs. 6a and 6b) (Sigman et al., 1999a; DiFiore et al., 2010; Smart et al., 2015; Kemeny et al., 2016). Lateral exchange with waters harboring a lower NO_3^- $\delta^{15}N$/(ln[NO_3^-]) relationship than CDW has been put forward to explain the OAZ T_{min} $\delta^{15}N$ anomaly (DiFiore et al., 2010). Exchange of AASW between the PAZ and OAZ was suggested to be the most likely candidate. However, a similar albeit weaker anomaly in $\delta^{15}N$ is also observed in the PAZ, arguing that lateral exchange cannot be the only process at play. Remineralization of low-$\delta^{15}N$ PN represents an alternative hypothesis (Sigman et al.,

1999a; Smart et al., 2015). It has been suggested that regenerated NO_3^- with a much lower $\delta^{15}N$ (~ -5 ± 5‰) than expected from NO_3^- assimilation is required to explain the T_{min} anomaly (Smart et al., 2015). Low suspended PN $\delta^{15}N$ has been reported for the Antarctic Zone (-4 to -2‰) (Altabet and Francois, 1994, 2001), with values as low as -5‰ observed in late summer in the Polar Frontal Zone (Lourey et al., 2003). The low PN $\delta^{15}N$ in late summer is likely due to the assimilation of regenerated ^{14}N-rich ammonium (Altabet, 1988; Fawcett et al., 2011) but requires further investigation. When this low-$\delta^{15}N$ PN is regenerated to NO_3^- upon wintertime deep mixing, it lowers NO_3^- $\delta^{15}N$ throughout the (winter) mixed layer (Smart et al., 2015). A related possibility is that sinking PN is remineralized with net isotope fractionation as it is exported through the T_{min}, generating low- $\delta^{15}N$ NH_4^+ that is subsequently oxidized to NO_3^-; this possibility will be addressed in a separate manuscript.

Compared to the variations observed in downcore diatom-bound $\delta^{15}N$ records (up to ~4‰) (Robinson and Sigman, 2008; Studer et al., 2015), the NO_3^- $\delta^{15}N/(\ln[NO_3^-])$ anomaly is small (~< 0.5‰). Nevertheless, it may have repercussions for paleoceanographic reconstructions (Kemeny et al., 2018). Within AASW from the T_{min} upward, a strong negative linear correlation is observed for NO_3^- isotopes *vs*. $\ln([NO_3^-])$ (p-value < 0.001; $R^2 > 0.76$), indicating that the dominant biogeochemical process at play is NO_3^- assimilation, mostly occurring in the spring-summer with the shoaling of the mixed layer (Sigman et al., 1999a; DiFiore et al., 2010; Rafter et al., 2013). Thus, our AASW-based estimates of the isotope effect (described below) are not affected by the T_{min} $\delta^{15}N$ anomaly.

4.2.3. Estimating the isotope effect of nitrate assimilation in the Antarctic Zone

The "AASW average" isotope effects are calculated using the entire AASW dataset (Table 1). "Regional average" isotope effects are calculated using data from individual cruises (IO8S, P16S, P18S, and SANAE54) or from the distinct regional continental shelf settings of the NBP cruises (Dumont D'Urvilles Sea, Davis Sea, Prydz Bay, and Ross Sea). "Station average" isotope effects are estimated by first calculating the isotope effect for each station and then averaging these estimates for each cruise or regional setting. All estimates were calculated using Equation 4. The AASW $^{15}\varepsilon$ average (± 1sd) is estimated to be 5.2 ± 0.1‰, with the regional $^{15}\varepsilon$ averages varying from 3.2‰ to 5.9‰ (Table 1). A low $^{15}\varepsilon$ is reported for Dumont D'Urville Sea and Prydz Bay, both of which are characterized by small amplitudes of NO_3^- depletion (~ 1.7 µmol l^{-1}) and ^{15}N-enrichment (~0.3‰). These amplitudes are relatively close to the analytical precision (±2sd) at the time when the samples from the NBP cruises were measured. Excluding these two areas, the AASW $^{15}\varepsilon$ average (± 1sd) is 5.4 ± 0.2‰, with the regional $^{15}\varepsilon$ averages varying between 4.8‰ and 5.9‰. Consistent with the expected effect of NO_3^--NO_2^- interconversion, the $^{15}\varepsilon$ estimate is higher and more variable for NO_3^--only, with an AASW $^{15}\varepsilon$ average of

7.3 ± 0.3‰, which varies regionally from 6.2‰ to 8.4‰, similar to what has been reported previously for acidified samples from the OAZ and SAZ (Altabet and Francois, 2001; Karsh et al., 2003; DiFiore et al., 2006). We calculate values of $^{18}\varepsilon$ that are lower than $^{15}\varepsilon$, counter to expectations for NO_3^- assimilation (Granger et al., 2004, 2010; Rohde et al., 2015). No significant difference is observed between NO_3^-+NO_2^- (4.3 ± 0.1‰) and NO_3^--only (4.5 ± 0.2‰) $^{18}\varepsilon$ estimates. We interpret both estimates to be artificially low, likely as a result of the NO_3^--NO_2^- interconversion process.

Compared to the PAZ, the OAZ NO_3^- $\delta^{15}N$ *vs.* ln([NO_3^-]) relationship is indistinguishable in slope but is shifted upward by ~0.3‰ (Fig. 6), reflecting the $\delta^{15}N$ difference in the sources of NO_3^- to the AASW in the PAZ (LCDW) and OAZ (UCDW). Despite this offset, similar isotope effects are reported for the two zones (Table 2). Over the summer months, lateral transport is likely decoupled between the surface mixed layer and the T_{min} layer, which could bias the estimation of the isotope effect based on vertical profile data. For example, if PAZ surface waters are advected above the OAZ T_{min}, the isotope effect will be underestimated. To estimate the maximal bias associated with this decoupling, we first calculate the average NO_3^- concentration and $\delta^{15}N$ of the T_{min} and mixed layer for the PAZ and OAZ. An equal-volume mixture of PAZ and OAZ water is also considered for the T_{min}. Using this range of scenarios for T_{min} conditions (i.e., PAZ, OAZ and a mixture), we then re-estimate the isotope effects for both the OAZ and PAZ mixed layers (Table 2). The results show that lateral exchange between the OAZ and PAZ can significantly bias our estimates, but that the resulting isotope effects are still within the range of both the full and regional datasets. Accordingly, we cannot confidently assess whether lateral transport is occurring and affecting our results.

A second approach is to estimate the isotope effect for each station individually. Due to the analytical precision of 0.2‰ (±2sd), only the stations with a vertical isotopic gradient greater than 0.2‰ in the AASW are used. Regrouped by hydrographic surveys, the averages of these station-by-station estimates are not significantly different from the "regional average" isotope effects described above (Table 1). In addition, no significant relationship with MLD is observed (p-value > 0.32; $R^2 < 0.04$; Fig. 7), nor with sampling date (p-value > 0.34; $R^2 < 0.03$, data not shown).

By breaking the problem into a series of individual stations, where each station within each region can be described with the Rayleigh model (Eq. 4), our dataset admits one equation for each station with only two unknowns per region, which are the source NO_3^- concentration and $\delta^{15}N$. We use method of least-squares to solve for these two parameters given the calculated intercept of each profile in Rayleigh space. The least-square solutions for the more pelagic stations, for which both NO_3^-+NO_2^- and NO_3^--only $\delta^{15}N$ are available (P16S, P18S, IO8S, and SANAE54), are 29.6 ± 1.1 μmol l^{-1}, 5.2 ± 0.2‰, and 5.6 ± 0.3‰

for NO_3^- concentration, $NO_3^-+NO_2^-$ $\delta^{15}N$, and NO_3^--only $\delta^{15}N$, respectively. These values are indistinguishable from the mean (±1sd) T_{min} conditions inferred from the observations at these stations: 29.6 ± 1.9 µmol l^{-1}, 5.2 ± 0.3‰, and 5.4 ± 0.4‰. This analysis further confirms that the T_{min} conditions are likely to be representative of the source conditions to the summer AZ surface waters. By including the NPB cruises, which are more representative of coastal Antarctic conditions and for which only $NO_3^-+NO_2^-$ $\delta^{15}N$ is available, the least-square solutions are 26.8 ± 3.8 µmol l^{-1} and 5.6 ± 0.4‰ for NO_3^- concentration and $NO_3^-+NO_2^-$ $\delta^{15}N$, respectively. These values are in agreement with the lower T_{max} NO_3^- concentration (25.8 ± 3.0 µmol l^{-1}) and higher T_{max} $NO_3^-+NO_2^-$ $\delta^{15}N$ (5.9 ± 0.6‰) observed at these stations.

Averaging (± sd) both the regional and station $^{15}\varepsilon$ averages, we estimate a nitrate assimilation isotope effect of 5.5 ± 0.6‰ for the Antarctic Zone, based on the $NO_3^-+NO_2^-$ measurements (Table 1). An isotope effect of 7.8 ± 1.5‰ is derived from the NO_3^--only measurements; we interpret this to be artificially high due to the isotopic impacts of NO_3^--NO_2^- interconversion described above. The relative stability of the isotope effect calculated from $NO_3^-+NO_2^-$ measurements, as well as the absence of any correlation with MLD (Fig. 7a) are in disagreement with previous studies. Using a compilation of NO_3^- isotope data from the Australian sector of the Southern Ocean, DiFiore et al. (2010) observed a poleward decrease in $^{15}\varepsilon$ from the SAZ to the PAZ (i.e., from ~ 9‰ to 5‰). However, except for the PAZ dataset, the OAZ-SAZ estimates were derived from acidified samples (Sigman et al., 1999a; Altabet and Francois, 2001; Karsh et al., 2003; DiFiore et al., 2006). DiFiore et al. (2010) hypothesized that this variation was driven by the southward shoaling of the mixed layer (Fig. 1), consistent with culture evidence for a physiological response of NO_3^- assimilation and cellular NO_3^- efflux to light availability (Needoba et al., 2004). Given our new understanding of the role of NO_2^-, we now propose that the higher OAZ $^{15}\varepsilon$ estimates were due to NO_3^--NO_2^- interconversion, leading to higher apparent values of $^{15}\varepsilon$ driven by the subsequent loss of NO_2^- during acidified storage in the OAZ samples (Table 1; Figs. 6a, b) (Park and Lee, 1988; Rayson et al., 2012). The spatial variability of the MLD in the Antarctic Zone is significant (Fig. 1), and MLD is likely to have been significantly different during ice ages. Thus, our finding of no impact of MLD on $^{15}\varepsilon$ simplifies paleoceanographic interpretation of N isotope data in terms of the degree of NO_3^- consumption (Robinson and Sigman, 2008).

4.3. Comparison of nitrate-based $^{15}\varepsilon$ estimates with sinking PN $\delta^{15}N$ data

Based on the observed Rayleigh fractionation trend in the AASW $NO_3^-+NO_2^-$ data and the N isotope effect of NO_3^- consumption that we estimate from them (Table 1), we infer an exported PN $\delta^{15}N$ of ~0.4‰ (-0.2‰ to 1.3‰), which is in the range of the annual-weighted sinking PN $\delta^{15}N$ from sediment

traps in the Antarctic Zone, -0.1‰ to 1.7‰ (Altabet and Francois, 2001). In contrast, if NO_3^--only data are used to estimate $^{15}\varepsilon$, then the resulting export production $\delta^{15}N$ is too low (-4.4‰ to -0.2‰) given the constraints offered by the sediment trap data. This supports our argument that the $NO_3^-+NO_2^-$ pool is more representative of the N available for consumption and is thus the appropriate substrate pool from which to estimate $^{15}\varepsilon$. This is confirmed more broadly using sediment trap data from both the OAZ and the Polar Frontal Zone (Altabet and Francois, 2001; Lourey et al., 2003). To account for the effect of varying source NO_3^- concentration and $\delta^{15}N$, the difference between annual-weighted sinking PN $\delta^{15}N$ and initial $\delta^{15}N$ of NO_3^- is plotted against the degree of nitrate consumption (= 1-f) (Fig. 9) (Altabet and Francois, 2001). Estimates of the degree of nitrate consumption are based on winter to summer seasonal NO_3^- consumption, and initial NO_3^- $\delta^{15}N$ on winter observations in the mixed layer at the corresponding sediment trap locations. The values for both degree of nitrate consumption and initial NO_3^- $\delta^{15}N$ are given in Altabet and François (2001) and Lourey et al. (2003). Annual-weighted sinking PN $\delta^{15}N$ falls on the AASW Rayleigh fractionation trend for the accumulated product if the $^{15}\varepsilon$ estimated from the $NO_3^-+NO_2^-$ pool is used (Fig. 9); in contrast, the trend underestimates sinking PN $\delta^{15}N$ if the $^{15}\varepsilon$ estimated from the NO_3^--only data is used. This analysis confirms a tight connection between the degree of NO_3^- consumption and the $\delta^{15}N$ of (1) $NO_3^-+NO_2^-$ and (2) export production (Sigman et al., 1999a; Altabet and Francois, 2001).

4.4. Paleoceanographic implications

The strong and consistent relationship between $NO_3^-+NO_2^-$ concentration and $\delta^{15}N$, which yields a relatively constant isotope effect in the lower range of previous estimates (~ 5.5 $\pm$ 0.6‰; from 4.5‰ to 6.2‰, Table 1), has implications for reconstructions of the past degree of NO_3^- consumption and thus the NO_3^- concentration in Antarctic Zone surface waters (Table 3). The $\delta^{15}N$ of coral- and diatom-bound organic N in the Antarctic Zone during the last ice age was 4‰ higher than today (Sigman et al., 1999b; Robinson and Sigman, 2008; Studer et al., 2015; Wang et al 2017), indicating elevated nitrate consumption during glacial periods (François et al., 1997).

In order to apply our new isotope effect estimates to a sedimentary diatom frustule-bound $\delta^{15}N$ record from the Pacific sector covering the last two glacial cycles (Studer et al., 2015), we need to take into account an isotopic offset between diatom-bound and sinking PN $\delta^{15}N$, recognizing that bulk sinking PN is not entirely composed of diatoms and that diatom-bound N has a different isotopic composition from that of bulk diatom biomass (Sigman et al., 1999b; Brunelle et al., 2007; Robinson and Sigman, 2008; Horn et al., 2011a; Morales et al., 2014). We estimate the isotopic offset from the difference (~1.8‰)

between expected sinking PN $\delta^{15}N$ in the modern Antarctic Zone (~0.4‰) and core-top diatom-bound $\delta^{15}N$ (~2.2‰; Studer et al., 2015), and apply this correction to the down-core diatom-bound $\delta^{15}N$ record (Table 3). This isotopic offset is relatively consistent, with the mean $\delta^{15}N$ offset reported for sinking PN and core-top diatom-bound $\delta^{15}N$ in high-latitude regions (2‰ to 4‰) (Brunelle et al., 2007; Robinson and Sigman, 2008) and for net-collected bulk organic matter and diatom-bound N in the sea-ice covered water column of the Bering Shelf (2.6 $\pm$ 2.5‰) (Morales et al., 2014). A similar offset (~3‰) was also recovered in a frustule cleaning study of diatoms grown for aquaculture (Morales et al., 2011), while a culture study of various species of diatoms yielded a range of offsets (Horn et al., 2011a). The higher isotope effect range suggested by NO_3^--only measurements predicts lower expected sinking PN $\delta^{15}N$ (-2.1‰) and thus requires a larger isotopic offset (4.3‰) to simulate the core-top diatom-bound $\delta^{15}N$. Changes in diatom assemblage between glacial and interglacial periods are relatively modest in the investigated record (Studer et al 2015), implying little effect from interspecies variability on the frustule-biomass isotopic offset that may be important in other down-core records from the Atlantic sector of the Antarctic Zone (Jacot des Combes et al., 2008; Horn et al., 2011b). This is further supported by assemblage-specific measurements of diatom-bound $\delta^{15}N$ through this record (Studer et al., 2015). However, the controls on the frustule-biomass isotopic offset remain unclear, requiring further study.

Taking into account the variability encountered in the modern Antarctic Zone for the source NO_3^- $\delta^{15}N$ and isotope effect, we infer that the degree of NO_3^- consumption increased by ~60-80% during ice ages (Fig. 10; Table 3). The higher isotope effect range estimated from NO_3^--only and acidified samples suggests a weaker increase (~30-65%). Our study suggests that the higher isotope effects implied by the NO_3^--only and acidified samples are likely an artifact derived from mixed layer NO_3^--NO_2^- interconversion, which argues for lower ice age Antarctic surface NO_3^- concentrations (< 7 µmol l^{-1}) than would have been calculated using the previous best estimates for $^{15}\varepsilon$ in the Antarctic Zone (< 15 µmol l^{-1}; Table 3). A separate issue is the suitability of the Rayleigh model for simulating ice age Antarctic conditions; this is addressed elsewhere (Kemeny et al., 2018).

4.5. Isotope effects from different oceanic regions

If the isotope effect estimates from NO_3^--only data in the high-latitude regions are discarded, our estimate for the isotope effect of nitrate assimilation in the Antarctic Zone (5.5 $\pm$ 0.6‰) is similar to estimates based on the NO_3^- concentration/$\delta^{15}N$ relationship in other oceanic regions (Table 4), particularly for nutrient-replete environments (4.5-6.7‰). Large variations in the MLD in high-latitude regions may provide a mechanism by which subsurface communities of nitrifying microorganisms are entrained into the mixed layer, leading to conditions favorable for NO_3^--NO_2^- interconversion and thus a

higher NO_3^--only $^{15}\varepsilon$ than expected from NO_3^- assimilation alone. In the Subantarctic Zone, this is supported by new measurements showing NO_2^- $\delta^{15}N$ as low as -52 $\pm$ 11‰ in the mixed layer of the GOSHIP IO8S and P18S sections (data not shown). In the subarctic Pacific, this hypothesis is supported by much lower NO_3^-+NO_2^- $^{15}\varepsilon$ (4.7-5.5‰) (Brunelle, 2009) than for NO_3^--only $^{15}\varepsilon$ (5.8-9.1‰) (Altabet and Francois, 1994b; Wu et al., 1997).

In lower latitude regions, NO_3^--only $^{15}\varepsilon$ appears to be more representative than NO_3^-+NO_2^- $^{15}\varepsilon$ of the 'true' isotope effect for NO_3^- assimilation (Table 3) (Fawcett et al., 2015; Rafter and Sigman, 2016), in which case the former could be compared with $^{15}\varepsilon$ estimates from acidified samples in similar environments (Altabet et al., 1999). The evidence in favor of this view is that (1) NO_3^--only (rather than NO_3^-+NO_2^-) $\delta^{15}N$ and $\delta^{18}O$ increase in unison from below the euphotic zone toward the surface, in agreement with NO_3^- assimilation, and (2) NO_2^- $\delta^{15}N$ is higher than in AASW and thus less clearly affected by NO_3^--NO_2^- interconversion (Fawcett et al., 2015; Rafter and Sigman, 2016; Peng et al., 2018). The implication is that, rather than being strongly influenced by NO_3^--NO_2^- interconversion, the $\delta^{15}N$ of NO_2^- at the lower latitude regions is dominantly altered by other NO_2^--oxidizing and -reducing processes. In nutrient-depleted regions, the $^{15}\varepsilon$ estimates tend to be lower and more variable (Table 3). We cannot rule out underestimation of the isotope effect due to artifacts from mixing in these settings. However, culture studies report systematically lower isotope effects (< 5‰) for haptophytes, chlorophytes and cyanobacteria, which are the phytoplankton groups that are known to prevail in these environments (Montoya and McCarthy, 1995; Granger et al., 2010). Alternatively, at adequately low [NO_3^-], there may be a reduction in the $^{15}\varepsilon$ of a given phytoplankton strain (Granger et al., 2004).

The subarctic North Atlantic is characterized by little difference in $\delta^{15}N$ and $\delta^{18}O$ between NO_3^-+NO_2^- and NO_3^--only (Peng et al., 2018), yielding $^{15}\varepsilon$ estimates of 5.2‰ to 5.3‰ and 5.1‰ to 5.2‰, respectively. In this environment, NO_2^- dynamics thus appear to be relatively unimportant in the isotope dynamics. [NO_2^-] is not at appreciably lower concentration through the upper water column than in the Antarctic (Peng et al., 2018). Thus, in the subarctic North Atlantic, NO_2^- $\delta^{15}N$ must be far less distinct from NO_3^-. One possible explanation is that mixed layer depth is less variable subsequent to spring/summer mixed layer shoaling, leading to less entrainment of nitrifiers into the euphotic zone and thus an overall lack of the isotopic processing that applies in the summertime Antarctic.

The overall stability of the isotope effect in nutrient-replete regions (4.5‰ to 6.7‰) contrasts with the large range of values reported from culture studies (~1‰ to 20‰) and the expected variations induced by changing NO_3^- metabolisms (Montoya and McCarthy, 1995; Granger et al., 2004, 2010; Needoba et al., 2004; Karsh et al., 2012, 2014). NO_3^- assimilation has been conceptualized as a stepwise process, in

which NO_3^- is actively taken up through the membrane into the cell (i.e., NO_3^- uptake, $^{15}\varepsilon_{upt} \sim 2‰$; Karsh et al., 2014). Once inside the cell, NO_3^- can either be reduced by the nitrate reductase enzyme, which is thought to be the dominant fractionating step ($^{15}\varepsilon_{NR} \sim 26.6‰$) or released back into the surrounding water with the isotope effect of NO_3^- efflux ($^{15}\varepsilon_{eff} \sim 1.2‰$) (Karsh et al., 2012, 2014). Any imbalance between NO_3^- uptake and intracellular reduction allows ^{15}N-enriched NO_3^-, which is accumulated inside the cell (e.g., in the vacuole), to be released via NO_3^- efflux, transmitting the ^{15}N-enrichment to seawater NO_3^- (Needoba et al., 2004). Given the enzyme-level isotope effects available in the literature, the organism-level isotope effect lies between ~ 2‰ ($^{15}\varepsilon_{upt}$) and ~ 25.8‰ ($^{15}\varepsilon_{upt} + {}^{15}\varepsilon_{NR} - {}^{15}\varepsilon_{eff}$) for an efflux/uptake ratio of 0 and 1, respectively (Karsh et al., 2012, 2014). An isotope effect between 4.5‰ and 6.7% argues for a small and relatively constant (0.10-0.27) efflux/uptake ratio in nutrient-replete regions (Table 3), with the caveat that the isotope effect provides an integrative measure of seasonal NO_3^- consumption and therefore a succession of different phytoplankton assemblages and NO_3^- metabolisms. Lower isotope effects in nutrient-depleted regions may point to an efflux/uptake ratio less than 0.05, with most of the isotope fractionation driven by NO_3^- uptake. However, as described above, we cannot rule out underestimation of the isotope effect due to artifacts resulting from mixing in these low-nutrient settings.

Conclusions and remaining questions

We report a relatively constant isotope effect for summertime NO_3^- assimilation in the modern Antarctic Zone ($5.5 \pm 0.6‰$), representative of the full seasonal NO_3^- depletion and the associated range of physical properties encountered in this region of the Southern Ocean. This implies a tight connection between the degree of NO_3^- consumption and the $\delta^{15}N$ of both the NO_3^- pool and the export flux. These findings contradict previous studies that reported variability in the isotope effect due to varying environmental conditions (i.e. mixed layer depth), and simplify the effort to reconstruct the degree of NO_3^- consumption in the Antarctic Zone at times in the past.

We suggest that the variability reported in previous studies is due to a methodological artifact, induced by putative NO_3^--NO_2^- interconversion in the mixed layer. Although the systematics of NO_3^--NO_2^- interconversion are relatively straightforward for the N isotopes, operating as a closed system where N atoms are exchanged between NO_3^- and NO_2^- and expressing a large equilibrium N isotope effect, the systematics applicable to the O isotopes remain unknown. No clear difference is reported between NO_3^--NO_2^- and NO_3^--only $\delta^{18}O$. However, the small contribution ($0.7 \pm 0.2\%$) of NO_2^- to the NO_3^-+NO_2^- pool may mask large differences in NO_2^- $\delta^{18}O$ (~50‰) that yield no significant differences ($\pm$ 0.2‰) in NO_3^-

+NO_2^- and NO_3^--only $\delta^{18}O$. Kinetic isotope effects during the incorporation and removal of O atoms are expected, as well as equilibrium isotope effects between NO_3^- and NO_2^- as well as between NO_3^--NO_2^- and water. However, the full elucidation of these systematics requires the measurement of the $\delta^{18}O$ of NO_2^- immediately upon sample collections (e.g., Buchwald et al., 2015).

Another open question for future studies concerns the higher N isotope effect estimates previously reported for the Subantarctic Zone, also based on measurements from acidified samples (DiFiore et al., 2006; 2010). It remains possible that the particularly deep mixed layers of the SAZ are adequate for light limitation to cause a higher $^{15}\varepsilon$ for nitrate assimilation, as observed in culture experiments (Needoba et al., 2004). However, new measurements of both NO_3^-+NO_2^- and NO_3^--only $\delta^{15}N$ on the GOSHIP IO8S and P18S sections indicate that NO_3^--NO_2^- interconversion also occurs in the SAZ mixed layer, with NO_2^- $\delta^{15}N$ estimated to be as low as -52 $\pm$ 11‰ (data not shown). Thus, artifacts related to NO_2^- loss during storage have likely also raised the measured NO_3^- $\delta^{15}N$ and thus the estimates of $^{15}\varepsilon$ in this zone of the Southern Ocean as well. A model taking into account the NO_3^- supplies from both the south and the underlying SAZ thermocline is required to tackle this question.

Acknowledgments

The new stable isotope data for the GOSHIP section IO8S and P18S presented in this study will be merged into the IO8S and P18S CCHDO product (https://cchdo.ucsd.edu/). We thank the ship captains, crews, and chief scientists (R.V. Roger Revelle, R.V. Ronald H. Brown, and R.V. SA Agulhas II) who supported the sampling activities during the various field programs that contributed to this study. We are also grateful to M.A. Weigand (Princeton University) for methodological advice and Barbara Hinnenberg (MPIC) for help with sample processing. This study was funded by the Max Planck Society. SEF thanks the South African National Research Foundation and Antarctic Programme (through grants 105539 and 110735). DMS acknowledges US NSF grant 1401489, as well as 0960802, 0992345, 0612198. P.C.K. acknowledges support from the Fannie & John Hertz Foundation and the Department of Defense NDSEG Fellowship.

References

Abernathey R. and Ferreira D. (2015) Southern Ocean isopycnal mixing and ventilation changes driven by winds. *Geophys. Res. Lett*. **43**, 10357-10365, doi:10.1002/2015GL066238.

Altabet M.A. (1988) Variations in nitrogen isotopic composition between sinking and suspended particles: implications for nitrogen cycling and particle transformation in the open ocean. *Deep-Sea Res*. **35(4)**, 535-554.

Altabet M.A. and Francois R. (1994a) Sedimentary nitrogen isotopic ratio as a recorder for surface ocean nitrate utilization. *Global Biogeochem. Cy*. **8(1)**, 103-116.

Altabet M.A. and Francois R. (1994b) The use of nitrogen isotopic ratio for reconstruction of past change in surface ocean nutrient utilization, p. 281-306. In R. Zahn, M. Kaminski, L. Labeyrie, and T.F. Pederson (eds.), Carbon cycling in the glacial ocean: Constraints on the ocean's role in global change, Springer-Verlag.

Altabet M.A., Pilskaln C., Thunell R., Pride C., Sigman D.M., Chavez F., and François R. (1999) The nitrogen isotope biogeochemistry of sinking particles from the margin of the Eastern North Pacific. *Deep Sea Res. I* **46**, 655-679.

Altabet M.A. and Francois R. (2001) Nitrogen isotope biogeochemistry of the Antarctic Polar Frontal Zone at 170°W. *Deep-Sea Res. II* **48**, 4247-4273.

Altabet M.A. (2001) Nitrogen isotopic evidence for micronutrient control of fractional NO_3^- utilization in the equatorial Pacific. *Limnol. Oceanogr*. **46(2)**, 368-380.

Böhlke J.K., Mroczkowski S.J. and Coplen T.B. (2003) Oxygen isotopes in nitrate: new reference materials for ^{18}O:^{17}O:^{16}O measurements and observations on nitrate-water equilibration. *Rapid Commun. Mass Spectrom*. **17**, 1835-1846.

Brunelle B.G., Sigman D.M., Cook M.S., Keigwin L.D., Haug G.H., Plessen B., Schettler G. and Jaccard S.L. (2007) Evidence from diatom-bound nitrogen isotopes for subarctic Pacific stratification during the last ice age and a link to North Pacific denitrification changes. *Paleoceanography* **22**, PA1215, doi:10.1029/2005PA001205.

Brunelle B.G. (2009) Nitrogen isotope constraints on the biogeochemistry and paleoclimatology of the Subarctic North Pacific. Ph.D. Thesis, Princeton Univ.

Brunner B., Contreras S., Lehmann M.F., Matantseva O., Rollog M., Kalvelage T., Klockgether G., Lavik G., Jetten M.S.M., Kartal B. and Kuypers M.M.M. (2013) Nitrogen isotope effects induced by anammox bacteria. *PNAS* **110**(47): 18994-18999.

Buchwald C., Santoro A.E., McIlvin M.R. and Casciotti K.L. (2012) Oxygen isotopic composition of nitrate and nitrite produced by nitrifying cocultures and natural marine assemblages. *Limnol. Oceanogr.* **57(5)**, 1361-1375.

Buchwald C., Santoro A.E., Stanley R.H.R. and Casciotti K.L. (2015) Nitrogen cycling in the secondary nitrite maximum of the eastern tropical North Pacific off Costa Rica. *Global Biogeochem. Cycles* **29**: 2061-2081, doi:10.1002/2015GB005187.

Casciotti K.L., Sigman D.M., Galanter M., Hasting M., Böhlke J.K. and Hilkert A. (2002) Measurement of the oxygen isotopic composition of nitrate in seawater and freshwater using the denitrifier method. *Anal. Chem.* **74**, 4905-4912.

Casciotti K.L., Trull T.W., Glover D.M. and Davies D. (2008) Constraints on nitrogen cycling at the subtropical North Pacific Station ALOHA from isotopic measurements of nitrate and particulate nitrogen. Deep-Sea Res. II **55**, 1661-1672.

Casciotti K.L. (2009) Inverse kinetic isotope fractionation during bacterial nitrite oxidation. *Geochim. Cosmochim. Acta* **73(7)**, 2061-2076, doi:10.1016/j.gca.2008.12.022.

DiFiore P.J., Sigman D.M., Trull T.W., Lourey M.J., Karsh K., Cane G. and Ho R. (2006) Nitrogen isotope constraints on subantarctic biogeochemistry. *J. Geophys. Res*. **111**, C08016,doi:10.1029/2005JC003216.

DiFiore P.J., Sigman D.M. and Dunbar R.B. (2009) Upper ocean nitrogen fluxes in the Polar Antarctic Zone: Constraints from the oxygen and nitrogen isotopes of nitrate. *Geochem. Geophys. Geosyst*. **10**, Q11016, doi:10.1029/2009GC002468.

DiFiore P.J., Sigman D.M., Karsh K.L., Trull T.W., Dunbar R.B. and Robinson R.S. (2010) Poleward decrease in the isotope effect of nitrate assimilation across the Southern Ocean. *Geophys. Res. Lett.* **37**, L17601, doi:10.1029/2010GL044090.

Dong S., Sprintall J., Gille S.T. and Talley L. (2008) Southern Ocean mixed-layer depth from Argo float profiles. *J. Geophys. Res.* **113**, CO6013, doi:10.1029/2006JC004051.

Fawcett S.E., Lomas M.W., Casey J.R., Ward B.B. and Sigman D.M. (2011) Assimilation of upwelled nitrate by small eukaryotes in the Sargasso Sea. *Nature Geoscience* **4**, doi:10.1038/NGEO01265.

Fawcett S.E., Ward B.B., Lomas M.W. and Sigman D.M. (2015) Vertical decoupling of nitrate assimilation and nitrification in the Sargasso Sea. *Deep-Sea Res. I* 103, 64-72.

Francois R., Altabet M.A., Yu E.-F., Sigman D.M., Bacon M.P., Frank M., Bohrmann G., Bareille G. and Labeyrie L.D. (1997) Contribution of Southern Ocean surface-water stratification to low atmospheric CO2 concentration during the last glacial period. *Nature* **389**, 929-935.

Friedman S.H., Massefki Jr. W. and Hollocher T.C. (1986) Catalysis of intermolecular oxygen atom transfer by nitrite dehydrogenase of *Nitrobacter agilis*. *J. Biol. Chem*. **261**(23): 10538-10543.

Fripiat F., Cavagna A.-J., Dehairs F., de Brauwere A., André L. and Cardinal D. (2012) Processes controlling the Si-isotopic composition in the Southern Ocean and application for paleoceanography. *Biogeosciences* **9**, 2443-2457.

Fripiat F., Sigman D.M., Fawcett S.E., Rafter P.A., Weigand M.A. and Tison J.-L. (2014) New insights into sea ice nitrogen biogeochemical dynamics from the nitrogen isotopes. *Global Biogeochem. Cy*. **28**, doi:10.1002/2013GB004729.

Fripiat F., Sigman D.M., Massé G. and Tison J.-L. (2015a) High turnover rates indicated by changes in the fixed N forms and their stable isotopes in Antarctic landfast sea ice. *J. Geophys. Res. Oceans* **120**, doi:10.1002/2014JC010583.

Fripiat F., Elskens M., Trull T.W., Blain S. et al. (2015b) Significant mixed layer nitrification in a natural iron-fertilized bloom of the Southern Ocean. *Global Biogeochem. Cy*. **29**, doi:10.1002/2014GB005051.

Granger J., Sigman D.M., Needoba J.A. and Harrison P.J. (2004) Coupled nitrogen and oxygen isotope fractionation of nitrate during assimilation by cultures of marine phytoplankton. *Limnol. Oceanogr*. **49(5)**, 1763-1773.

Granger J. and Sigman D.M. (2009) Removal of nitrite with sulfamic acid for nitrate N and O isotope analysis with the denitrifier method. *Rapid Commun. Mass Spectrom.* **23**, 3753-3762.

Granger J., Sigman D.M., Rohde M.M., Maldonado M.T. and Tortell P.D. (2010) N and O isotope effects during nitrate assimilation by unicellular prokaryotic and eukaryotic plankton cultures. *Geochim. Cosmochim. Acta* **74**, 1030-1040.

Holte J., Talley L.D., Gilson J. and Roemmich D. (2017) An Argo mixed layer climatology and database. *Geophys. Res. Lett*. **44**, 5618-5626, doi:10.1002/2017GL073426.

Horn M.G., Robinson R.S., Rynearson T.A. and Sigman D.M. (2011a) Nitrogen isotopic relationship between diatom-bound and bulk organic matter of cultured polar diatoms. *Paleoceanogr.* **26**, PA3208, doi:10.1029/2010PA002080.

Horn M.G., Robinson R.S., Rynearson T.A. and Sigman D.M. (2011b) Nitrogen isotopic relationship between diatom-bound and bulk organic matter of cultured polar diatoms. *Paleoceanogr.* **26**, PA3208, doi:10.1029/2010PA002080.

Jaccard S.L., Hayes C.T., Martinez-Garcia A., Hodell D.A., Anderson R.F., Sigman D.M. and Haug G.H. (2013) Two modes of change in Southern Ocean productivity over the past million years. *Science* **339**, 1419-1423.

Jacot Des Combes H., Esper O., De La Rocha C.L., Abelmann A., Gersonde R., Yam R. and Shemesh A. (2008) Diatom $\delta^{13}C$, $\delta^{15}N$, and C/N since the Last Glacial Maximum in the Southern Ocean: Potential impact of species composition. *Paleoceanogr.* **23**, PA4209, doi:10.1029/2008PA001589.

Karsh K.L., Trull T.W., Lourey M.J. and Sigman D.M. (2003) Relationship of nitrogen isotope fractionation to phytoplankton size and iron availability during the Southern Ocean Iron Release Experiment (SOIREE). *Limnol. Oceanogr.* **48(3)**, 1058-1068.

Karsh K.L., Granger J., Kritee K. and Sigman D.M. (2012) Eukaryotic Assimilatory Nitrate Reducase fractionates N and O isotopes with a ratio near unity. *Environ. Sci. Technol*. **46**, 5727-5735.

Karsh K.L., Trull T.W., Sigman D.M., Thompson P.A. and Granger J. (2014) The contributions of nitrate uptake and efflux to isotope fractionation during algal nitrate assimiation. *Geochim. Cosmochim. Acta* **132**, 391-412.

Kemeny P.C., Weigand M.A., Zhang R., Carter B.R., Karsh K.L., Fawcett S.E. and Sigman D.M. (2016). Enzyme-level interconversion of nitrate and nitrite in the fall mixed layer of the Antarctic Ocean. *Global Biogeochem. Cy*. **30**, 1069-1085, doi:10.1002/2015GB005350.

Kemeny P.C., Kast E.R., Hain M.P., Fawcett S.E., Fripiat F., Studer A.S., Martinez-Garcia A., Haug G.H. and Sigman D.M. (2018) A seasonal model of nitrogen isotopes in the ice age Antarctic Zone: Support for reduced upper cell overturning. Submitted to *Paleoceanography and Paleoclimatology*.

Kohfeld K.E., Le Quéré C., Harrison S.P. and Anderson R.F. (2005) Role of marine biology in glacial-interglacial CO_2 cycles. *Science* **308**, 74-78.

Lomas M.W. and Lipschultz F. (2006) Forming the primary nitrite maximum: nitrifiers or phytoplankton? *Limnol. Oceanogr*. **51**, 2453-2467.

Lourey M.J., Trull T.W. and Sigman D.M. (2003) Sensitivity of $\delta^{15}N$ of nitrate, surface suspended and deep sinking particulate nitrogen to seasonal nitrate depletion in the Southern Ocean. *Global Biogeochem. Cy*. **17(3)**, 1081, doi :10.1029/2002GB001973.

Mariotti A., Germon J.C., Hubert P., Kaiser P., Letolle R., Tardieux A. and Tardieux P. (1981) Experimental determination of nitrogen kinetic isotope fractionation: some principles; illustration for the denitrification and nitrification processes. *Plant and Soil* **62**, 413-430.

Marshall J. and Speer K. (2012) Closure of the meridional overturning circulation through Southern Ocean upwelling. *Nature Geoscience* **5**, doi:10.1038/NGEO1391.

Martin J.H., Gordon R.M. and Fitzwater S.E. (1990) Iron in Antarctic waters. *Nature* **345**, 156-158.

Martinez-Garcia A., Sigman D.M., Ren H., Anderson R.F., Straub M. S, Hodell D.A., Jaccard S.L., Eglinton T.I. and Haug G.H. (2014) Iron fertilization of the Subantarctic Ocean during the last ice age. *Science* **343**, 1347-1350.

McIlvin M.R. and Altabet M.A. (2005) Chemical conversion of nitrate and nitrite to nitrous oxide for nitrogen and oxygen isotopic analysis in freshwater and seawater. *Anal. Chem*. **77**, 5589-5595.

Mitchel B.G., Brody E.A., Holm-Hansen O., McClain C. and Bishop J. (1991) Light limitation of phytoplankton and macronutrient utilization in the Southern Ocean. *Limnol. Oceanogr.* **36**, 1662-1677.

Möbius J. (2013) Isotope fractionation during nitrogen remineralization (ammonification): Implications for nitrogen isotope biogeochemistry. *Geochim. Cosmochim. Acta* **105**, 422-432.

Montoya J.P. and McCarthy J.J. (1995) Isotopic fractionation during nitrate uptake by phytoplankton grown in continuous culture. *J. Plankton Res*. **17(3)**, 439-464.

Morales L.V., Granger J., Chang B.X., Prokopenko M.G., Plessen B., Gradinger R. and Sigman D.M. (2014) Elevated $^{15}N/^{14}N$ in particulate organic matter, zooplankton, and diatom frustule-bound nitrogen in the ice-covered water column of the Bering Sea eastern shelf. *Deep-Sea Res. II* **109**, 100-111.

Needoba J.A., Sigman D.M. and Harrison P.J. (2004) The mechanism of isotope fractionation during algal nitrate assimilation as illuminated by the $^{15}N/^{14}N$ of intracellular nitrate. *J. Phycol.* **40**, 517-522.

Orsi A.H., Whitworth III T. and Nowlin Jr. W.D. (1995) On the meridional extent and fronts of the Antarctic Circumpolar Current. *Deep-Sea Res. I* **42(5)**, 641-673.

Park J.-Y. and Lee Y.-N. (1988) Solubility and decomposition kinetics of nitrous acid in aqueous solution. *J. Phys. Chem.* **92**, 6294-6302.

Pellichero V., Sallée J.-B., Schmidtko S., Roquet F. and Charrassin J.-B. (2017) The ocean mixed layer under Southern Ocean sea-ice: Seasonal cycle and forcing. *J. Geophys. Res.* **122**, 1608-1633, doi:10.1002/2016JC011970.

Peng X., Fawcett S.E., van Oostende N., Wolf M.J., Marconi D., Sigman D.M. and Ward B.B. (2018) Nitrogen uptake and nitrification in the subarctic North Atlantic Ocean. In press in *Limnol. Oceanogr*., doi:10.1002/lno.10784.

Priscu J.C., Downes M.T., Priscu L.R., Palmisano A.C. and Sullivan C.W. (1990) Dynamic of ammonium oxidizer activity and nitrous oxide (N_2O) within and beneath Antarctic sea ice. *Mar. Ecol. Prog. Ser*. **62**, 37-46.

Rafter P.A., DiFiore P.J. and Sigman D.M. (2013) Coupled nitrogen and oxygen isotopes and organic matter remineralization in the Southern and Pacific Oceans. *J. Geophys. Res*. **118**, 1-14, doi:10.1002/jgrc.20316.

Rafter P.A. and Sigman D.M. (2016) Spatial distribution and temporal variation of nitrate nitrogen and oxygen isotopes in the upper equatorial Pacific Ocean. *Limnol. Oceanogr*. **61**, 14-31.

Raymond B. (2014) The maximum extent of sea ice in the southern hemisphere by day and winter season. Australian Data Center – CAASM Metadata (http://data.aad.gov.au/aadc/metadata/metadata_redirect.cfm?md=/AMD/AU/sea_ice_extent_winter).

Rayson M.S., Mackie J.C., Kennedy E.M. and Dlugogorski B.Z. (2012) Accurate rate constants for decomposition of aqueous nitrous acid. *Inorg. Chem*. **51**, 2178-2185.

Robinson R.S. and Sigman D.M. (2008) Nitrogen isotopic evidence for a poleward decrease in surface nitrate within the ice age Antarctic. *Quaternary Science Reviews* **27**, 1076-1090.

Rohde M.M., Granger J., Sigman D.M. and Lehmann M.F. (2008) Coupled nitrate N and O stable isotope fractionation by a natural marine plankton consortium. *Frontiers in Marine Science* **2**, 28, doi:10.3389/fmars.2015.00028.

Sarmiento J.L., Gruber N., Brzezinski M.A. and Dunne J.P. (2004) High-latitude controls of thermocline nutrients and low latitude biological productivity. *Nature* **427**, 56-60.

Sarmiento J.L., Simeon J., Gnanadesikan A., Gruber N., Key R.M. and Schlitzer R. (2007) Deep ocean biogeochemistry of silicic acid and nitrate. *Global Biogeochem. Cy*. **21**, GB1S90, doi:10.1029/2006GB002720.

Sigman D.M., Altabet M.A., McCorkle D.C., Francois R. and Fisher G. (1999a) The $\delta^{15}N$ of nitrate in the Southern Ocean: Consumption of nitrate in surface waters. *Global Biogeochem. Cy*. **13(4)**, 1149-1166.

Sigman D.M., Altabet M.A., Francois R., McCorkle D.C. and Gaillard J.-F. (1999) The isotopic composition of diatom-bound nitrogen in Southern Ocean sediments. *Paleoceanogr.* **14(2)**, 118-134.

Sigman D.M., Altabet M.A., McCorkle D.C., Francois R. and Fisher G. (2000) The $\delta^{15}N$ of nitrate in the Southern Ocean: Nitrogen cycling and circulation in the ocean interior. *J. Geophys. Res.* **105(C8)**, 19599-19614.

Sigman D.M., Casciotti K.L., Andreani M., Barford C., Galanter M. and Böhlke J.K. (2001) A bacterial method for the nitrogen isotopic analysis of nitrate in seawater and freshwater. *Anal. Chem*. **73**, 4145-4153.

Sigman D.M., DiFiore P.J., Hain M.P., Deutsch C., Wang Y., Karl D.M, Knapp A.N., Lehmann M.F. and Pantoja S. (2009a) The dual isotopes of deep nitrate as a constraint on the cycle and budget of oceanic fixed nitrogen. *Deep-Sea Res. I* **56**, 1419-1439.

Sigman D.M., DiFiore P.J., Hain M.P., Deutsch C., and Karl D.M. (2009b) Sinking organic matter spreads the nitrogen isotope signal of pelagic denitrification in the North Pacific. *Geophys. Res. Let*. **36**, L08605, doi:10.1029/2008GL035784.

Sigman D.M., Hain M.P. and Haug G.H. (2010) The polar ocean and glacial cycles in atmospheric CO_2 concentration. *Nature* **466**, doi:10.1038/nature09149.

Smart S.M., Fawcett S.E., Thomalla S.J., Weigand M.A., Reason C.J.C. and Sigman D.M. (2015) Isotopic evidence for nitrification in the Antarctic winter mixed layer. *Global Biogeochem. Cy.* **29**, doi:10.1002/2014GB005013.

Studer A.S., Sigman D.M., Martinez-Garcia A., Benz V., Winckler G., Kuhn G., Esper O., Lamy F., Jaccard S.L., Wacker L., Oleynik S., Gersonde R. and Haug G.H. (2015) Antarctic Zone nutrient conditions during the last two glacial cycles. *Paleoceanogr*. **30**, 845-862, doi:10.1002/2014PA002745.

Sundermeyer-Klinger H., Meyer W., Warninghoff B. and Bock E. (1984) Membrane-bound nitrite oxidoreductase of Nitrobacter: evidence for a nitrate reductase system. *Arch. Microbiol*. **140**, 153-158.

Talley L.D. (2013) Closure of the global overturning circulation through the Indian, Pacific, and Southern Oceans: Schematics and transports. *Oceanogr*. **26(1)**, 80-97.

Vanzella A., Guerrero M.A. and Jones R.D. (1989) Effect of CO and light on ammonium and nitrite oxidation by chemolithotrophic bacteria. *Mar. Ecol. Prog. Ser*. **57**, 69-76.

Wada E. and Hattori A. (1978) Nitrogen isotope effects in the assimilation of inorganic nitrogenous compounds by marine diatoms. *Geomicrobiol. J.* **1(1)**, 85-101.

Wang X.T., Sigman D.M., Prokopenko M.G., Adkins J.F., Robinson L.F., Hines S.K., Chai J., Studer A.S., Martinez-Garcia A., Chen T. and Haug G.H. (2017) Deep-sea coral evidence for lower Southern Ocean nitrate concentrations during the last ice age. *PNAS **114(13)***, 3352-3357.

Ward B.B. (1985) Light and substrate concentration relationship with marine ammonium assimilation and oxidation rates. *Mar. Chem*. **16**, 301-316.

Weigand M.A., Foriel J., Barnett B., Oleynik S. and Sigman D.M. (2016) Updates to instrumentation and protocols for isotopic analysis of nitrate by the denitrifier method. *Rapid Commun. Mass Spectrom.* **30(12)**, 1365-1383, doi:10.1002/rcm.7570.

Wu J., Calvert S.E. and Wong C.S. (1997) Nitrogen isotope variations in the subarctic northeast Pacific: relationships to nitrate utilization and trophic structure. *Deep-Sea Res. I* **44(2)**, 287-314.

Wunderlich A., Meckenstock R.U. and Einsiedl F. (2013) A mixture of nitrite-oxidizing and denitrifying microorganisms affects the $\delta^{18}O$ of dissolved nitrate during anaerobic microbial denitrification depending of the $\delta^{18}O$ of ambient water. *Geochim. Cosmochim. Acta* **119**: 31-45.

Zakem E.Z., Al-Haj A., Church M.J., van Dijken G.L., Dutkiewicz S., Foster S.Q., Fulweiler R.W., Mills M.M., and Follows M.J. (2018) Ecological control of nitrite in the upper ocean. *Nat. Commun*. **9**: 1206, doi:10.1038/s41467-018-03553-w.

Table captions

Table 1: Averages (± sd) for the isotope effects estimated by pooling different datasets (Eq. 4). The "AASW average" isotope effects are calculated using the entire AASW dataset. "Regional average" isotope effects are calculated using data from individual cruises (IO8S, P16S, P18S, and SANAE54) or from the distinct regional continental shelf settings of the NBP cruises (Dumont D'Urvilles Sea, Davis Sea, Prydz Bay, and Ross Sea). "Station average" isotope effects are estimated by first calculating the isotope effect for each station and then the average for each cruise or regional setting.

Table 2: The effect of varying PAZ and OAZ conditions for both the T_{min} and mixed layer on the N isotope effect (Eq. 4). In order to quantify this effect, we calculated the average NO_3^- concentration and $\delta^{15}N$ for both PAZ and OAZ T_{min} (column 1) and ML (column 2). A mixture between PAZ and OAZ (50-50%) is also considered for the T_{min}. These different conditions are inserted in Eq. 4 to calculate the N isotope effect for NO_3^-+NO_2^- and NO_3^-only (column 3 and 4, respectively).

Table 3: Surface NO_3^- utilization during the last glacial maximum inferred with both NO_3^-+NO_2^- and NO_3^-only $\delta^{15}N$ and $^{15}\varepsilon$, as well as variations in the parameters being used to estimate this values.

Table 4: Estimates of the isotope effects in different oceanic regions based on the relationship between NO_3^- concentration and $\delta^{15}N$.

Figure captions

Figure 1: Location of the stations (symbols) overlaid on mixed layer depth (MLD) climatology for February (Pellichero et al., 2017). The Polar Front (PF) and the Southern Antarctic Circumpolar Current Front (SACCF) according to Orsi et al. (1995) are indicated by the dashed and solid black lines, respectively. The solid and dashed white lines represent the mean winter maximal (WSI) and summer minimal (SSI) sea ice extent (1979-2008, ≥ 15% ice cover) (Raymond, 2014). The cyan inverted triangles indicate the stations for SANAE54, the orange triangles for P18S, the purple squares for P16S (Kemeny et al., 2016), the blue-green circles for IO8S, and the red stars for the NBP cruises (NBP01-1 and NBP06-8) (DiFiore et al., 2009).

Figure 2: Meridional depth sections of NO_3^- concentration (a), potential temperature (b), NO_3^-+NO_2^- $\delta^{15}N$ (c) and NO_3^-+NO_2^- $\delta^{18}O$ (d) in the Indian Sector at 78-95°E (IO8S). The thin white lines are contours of NO_3^- concentration (a), potential temperature (b), NO_3^-+NO_2^- $\delta^{15}N$ (c) and NO_3^-+NO_2^- $\delta^{18}O$ (d). The isopycnal delimiting Upper and Lower Circumpolar Deep Water is indicated with the thick black solid line. The sections were generated with Ocean Data View [Available at http://odv.awi.de].

Figure 3: Meridional depth sections of NO_2^- $\delta^{15}N$ (colored dots) with NO_2^- concentration overlay (black contours) for IO8S eastern Indian section (a), P18S eastern Pacific section (b), P16S western Pacific section (c) and SANAE54 Atlantic section (d). NO_2^- $\delta^{15}N$ is shown when the NO_2^- contribution to the NO_3^-+NO_2^- pool is larger than 0.25%. The black horizontal arrows above each panel indicate the Antarctic Zone. The sections were generated with Ocean Data View [Available at http://odv.awi.de].

Figure 4: Profiles of (a,b) NO_3^-+NO_2^- concentration, (c,d) NO_3^-+NO_2^- $\delta^{15}N$ and $\delta^{18}O$, and (d,e) NO_3^--only $\delta^{15}N$ and $\delta^{18}O$ for the Polar Antarctic Zone (PAZ) (a,c,e) and Open Antarctic Zone (OAZ) (b,d,f) for all stations. In the PAZ, the stations are grouped by their upper ocean thermohaline structure into three categories: 'T_{min}' stations (white circles), 'margin' stations (orange triangles) or 'T_{max}' stations (green-blue squares). The mean profiles for each category are given by the corresponding solid symbols (averages for 0-20, 20-40, 40-60, 60-80, 80-100, 100-125, 125-150, 150-200, 200-300, 300-400, and 400-500 m depth intervals). All stations in the OAZ fall into the T_{min} category.

Figure 5: Relationship between NO_3^-+NO_2^- and NO_3^--only $\delta^{15}N$ (a) and $\delta^{18}O$ (b). In (a), the black dots show the expected NO_3^- $\delta^{15}N$ if NO_2^- $\delta^{15}N$ was -35‰. This NO_2^- $\delta^{15}N$ value represents the minimum value expected from nitrification, NO_2^- assimilation, or an imbalance in assimilatory NO_3^- reduction (Fripiat et al., 2015a).

Figure 6: Relationship between $NO_3^-+NO_2^-$ (a,c) and NO_3^--only (b,d) concentrations and $\delta^{15}N$ (a,b) and $\delta^{18}O$ (c,d) for AASW (empty black circles and triangles for the PAZ and OAZ, respectively) and deep water (gray circles). Red triangles and blue circles correspond to the mean OAZ and PAZ profiles (averages for 0-20, 20-40, 40-60, 60-80, 80-100, 100-125, 125-150, 150-200, 200-300, 300-400, and 400-500 m depth intervals). Regressions for AASW are indicated with the black solid lines (AASW average in Table 1), and Rayleigh fractionation trends (with LCDW and UCDW as initial conditions) with the dashed colored lines (blue and red, respectively). The mean profiles for stations near the continental shelf (i.e., 'T_{max}' and 'margin' stations) are shown as green lines in (a) and (c), and are indistinguishable from the mean NO_3^- $\delta^{15}N/[NO_3^-]$ profiles at the more pelagic 'T_{min}' PAZ stations. In terms of NO_3^- $\delta^{18}O/[NO_3^-]$, the stations near the continental shelf have similar surface values to the pelagic PAZ stations, but with a lower NO_3^- $\delta^{18}O$ for a given NO_3^- concentration deeper in the water column (i.e., below ~ 140 m).

Figure 7: $^{15}\varepsilon$ (a) and $^{18}\varepsilon$ (b) vs. mixed layer depth (MLD) for $NO_3^-+NO_2^-$ (black circles) and NO_3^--only (black open circles). The solid line is for the average value of $NO_3^-+NO_2^-$ $^{15}\varepsilon$ (5.7‰) and $^{18}\varepsilon$ (4.4‰), and the dashed lines are for the average values of NO_3^--only $^{15}\varepsilon$ (8.4‰) and $^{18}\varepsilon$ (4.2‰) (station averages in Table 1). MLD was computed based on the threshold method with a finite-density difference criterion (0.03 kg m^{-3}) from near-surface reference values (Dong et al., 2008).

Figure 8: $^{15}\varepsilon$ vs. $^{18}\varepsilon$ for $NO_3^-+NO_2^-$ (gray circles) and NO_3^--only (gray open circles) (station averages in Table 1). NBP stations near and on the continental shelf are shown with the gray triangles (i.e., no NO_3^--only measurements). The averages are shown with larger corresponding black symbols and error bars. The solid line is for $^{15}\varepsilon = {}^{18}\varepsilon$.

Figure 9: Degree of nitrate consumption (= 1-f) *versus* the difference between annual sinking PN and NO_3^--source $\delta^{15}N$. Black circles show the annual-weighted sinking flux for the Antarctic Zone and white circles for the Polar Front Zone (Altabet and Francois, 2001; Lourey et al., 2003). The curved lines and shading denote AASW Rayleigh fractionation trends with varying isotope effects. The isotope effects for $NO_3^-+NO_2^-$ (mean = 5.5‰, varying from 4.5 to 6.2‰) are shown in orange and for NO_3^--only in blue-green (mean = 7.8‰, varying from 6.2 to 10.3‰) (Table 1).

Figure 10: Past degree of NO_3^- consumption (= 1-f) inferred from the AASW Rayleigh fraction trends (Fig. 6) for $NO_3^-+NO_2^-$ (orange) and NO_3^--only (green-blue) and a diatom-bound $\delta^{15}N$ record from the Pacific sector of the Antarctic Zone, corrected for a constant isotopic offset between diatom biomass and frustule-bound N (Studer et al., 2015). The isotopic offset is taken from difference between core-top diatom-bound $\delta^{15}N$ and the expected export production $\delta^{15}N$, inferred from the AASW Rayleigh accumulated product (Table 3). The source NO_3^- $\delta^{15}N$ (T_{min}) varies from 5.0 to 6.2‰ in the case of NO_3^-

$+NO_2^-$ and from 5.1 to 6.0‰ for NO_3^--only. The $^{15}\varepsilon$ varies from 4.5 to 6.7‰ in the case of $NO_3^-+NO_2^-$ and from 6.2 to 10.8‰ for NO_3^--only (Table 3). The dashed black and gray lines represent the mean fractional NO_3^- depletion implied by the $NO_3^-+NO_2^-$ and NO_3^--only isotope effects, respectively.

Figure A1: Meridional depth sections of NO_3^- concentration (a), potential temperature (b), $NO_3^-+NO_2^-$ $\delta^{15}N$ (c) and $NO_3^-+NO_2^-$ $\delta^{18}O$ (d) in the eastern Pacific Sector at ~ 100°W (P18S). The thin white lines are contours of NO_3^- concentration (a), potential temperature (b), $NO_3^-+NO_2^-$ $\delta^{15}N$ (c) and $NO_3^-+NO_2^-$ $\delta^{18}O$ (d). The isopycnal delimiting Upper and Lower Circumpolar Deep Water is indicated by the thick black solid line. The sections were generated with Ocean Data View [Available at http://odv.awi.de].

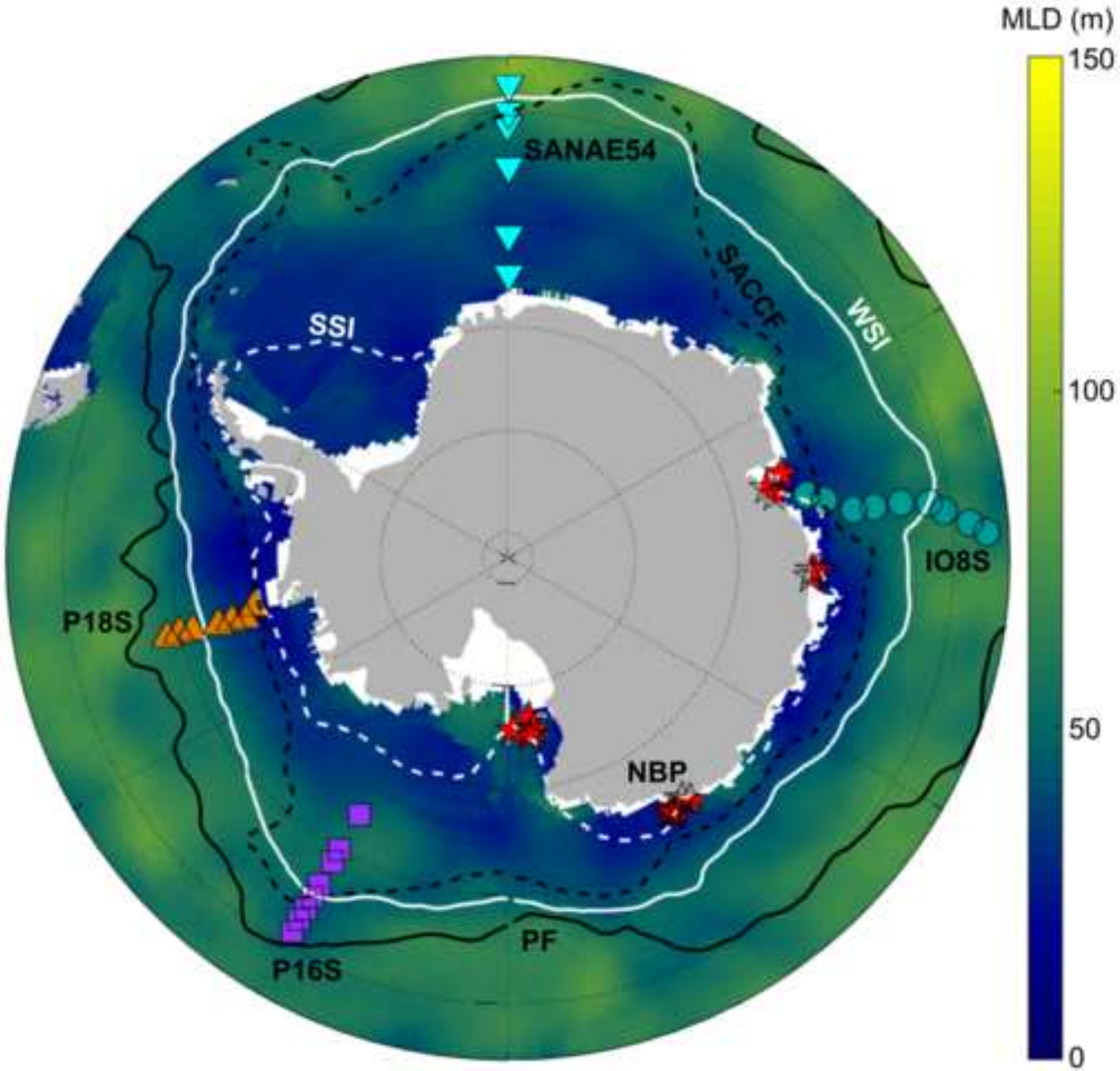

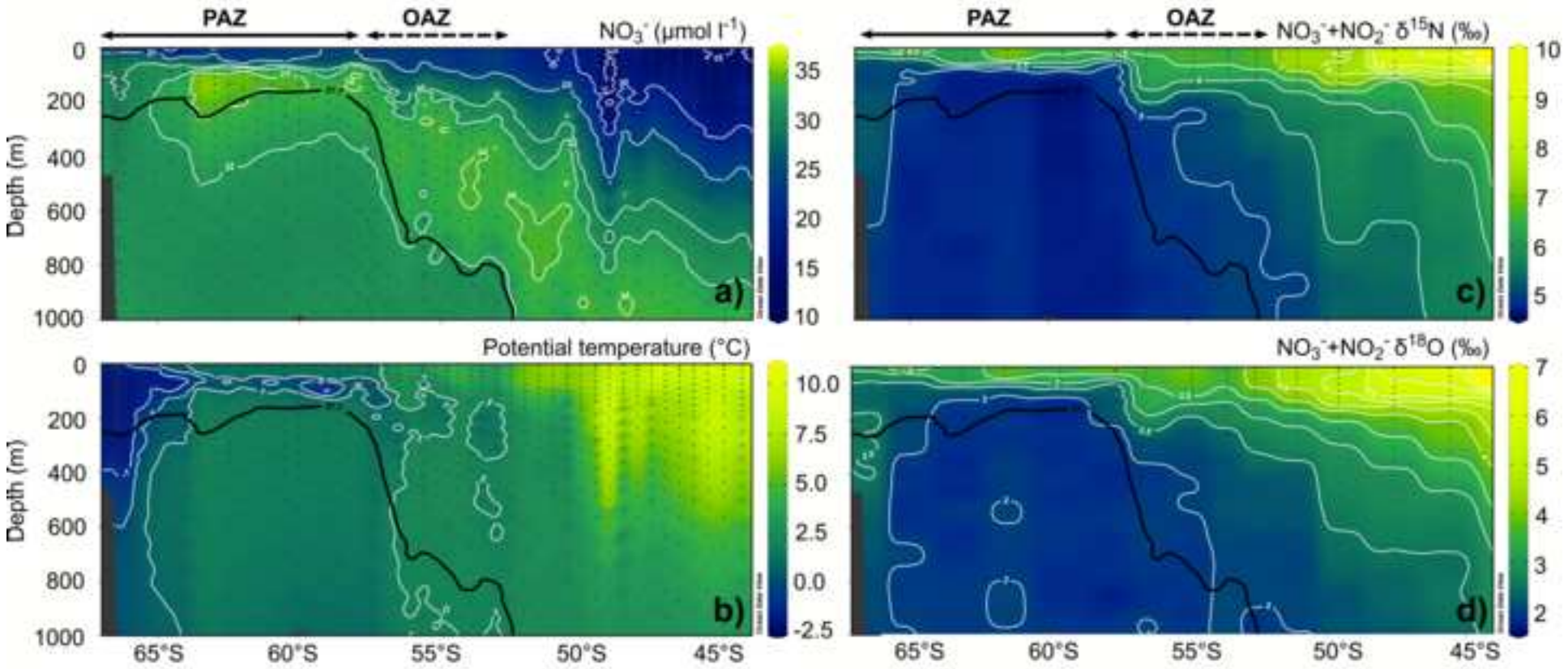

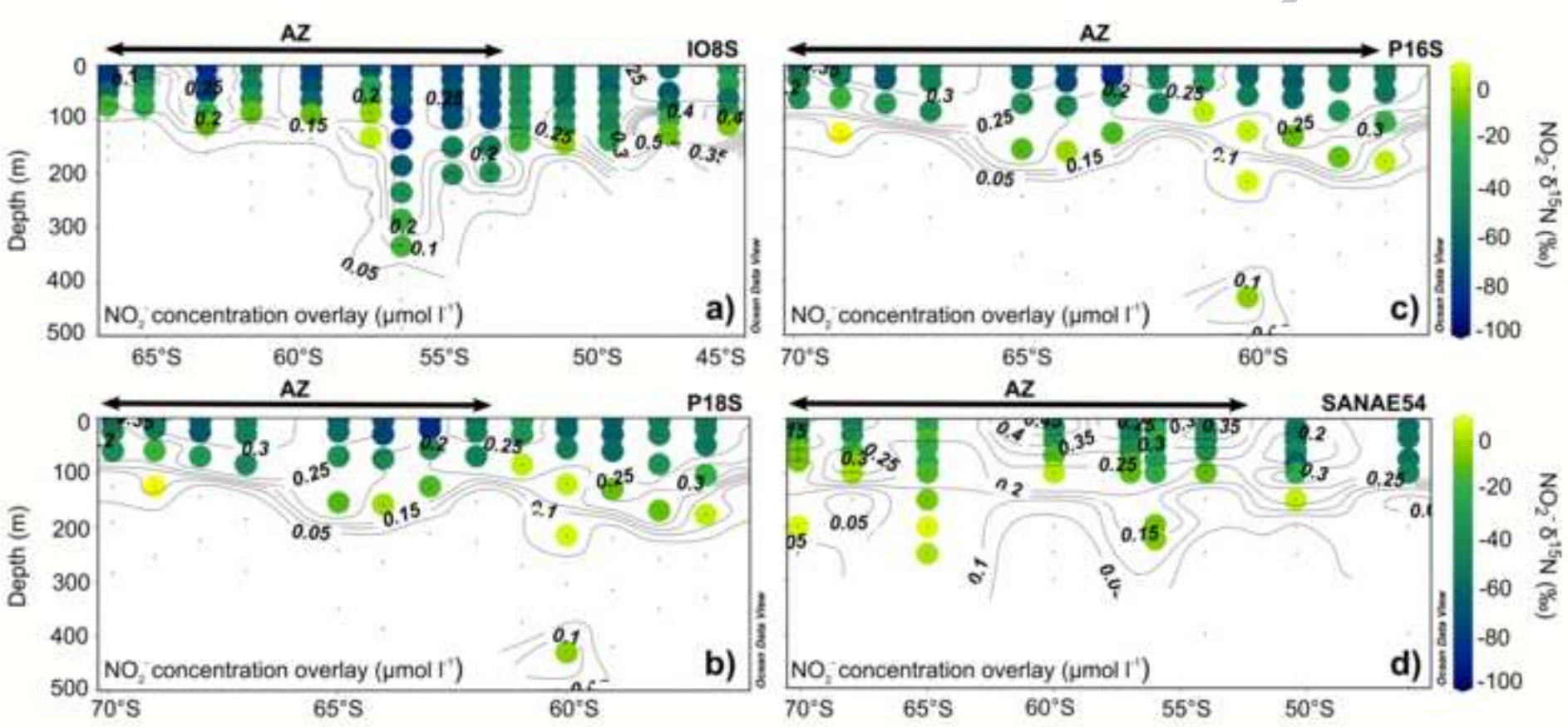

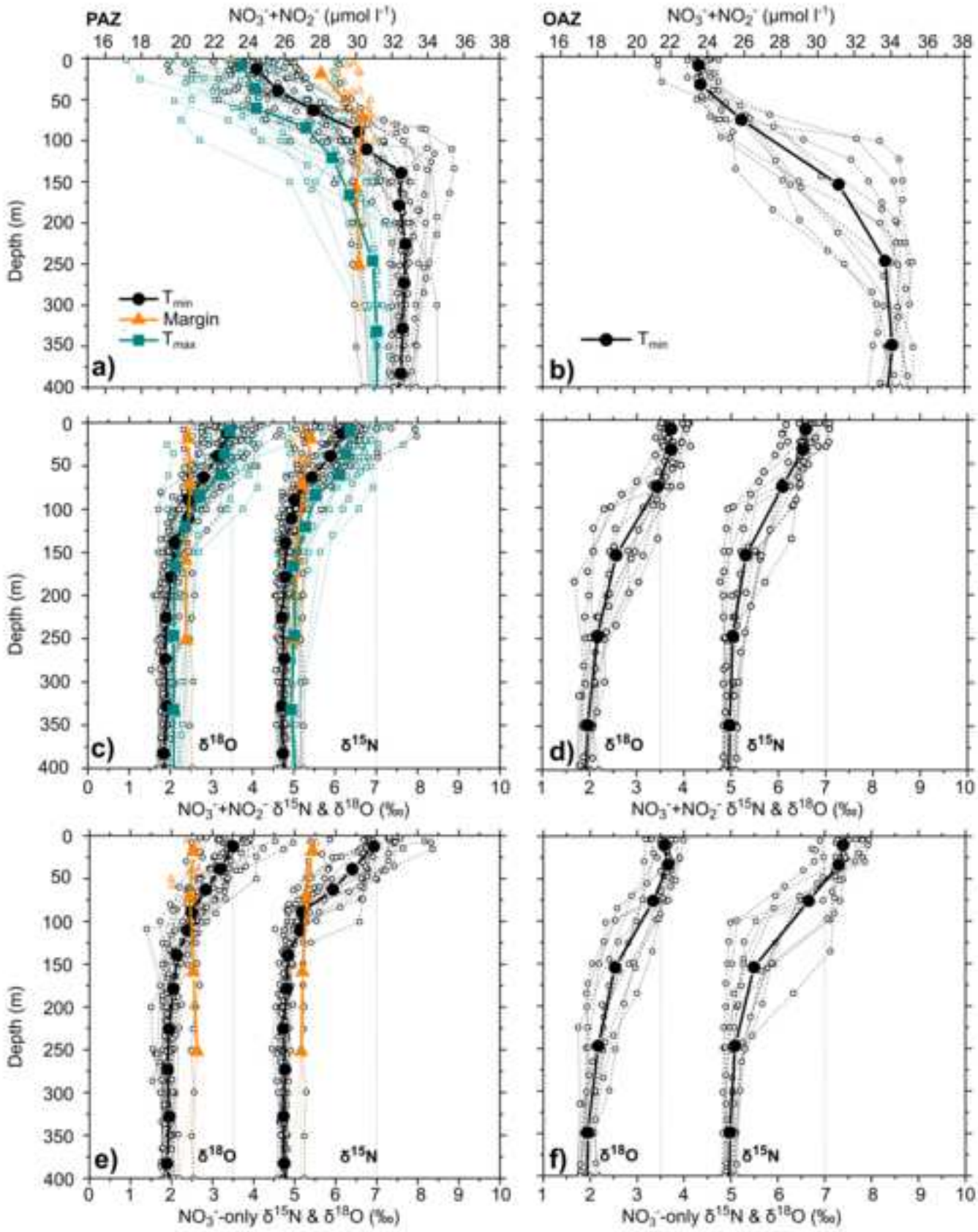

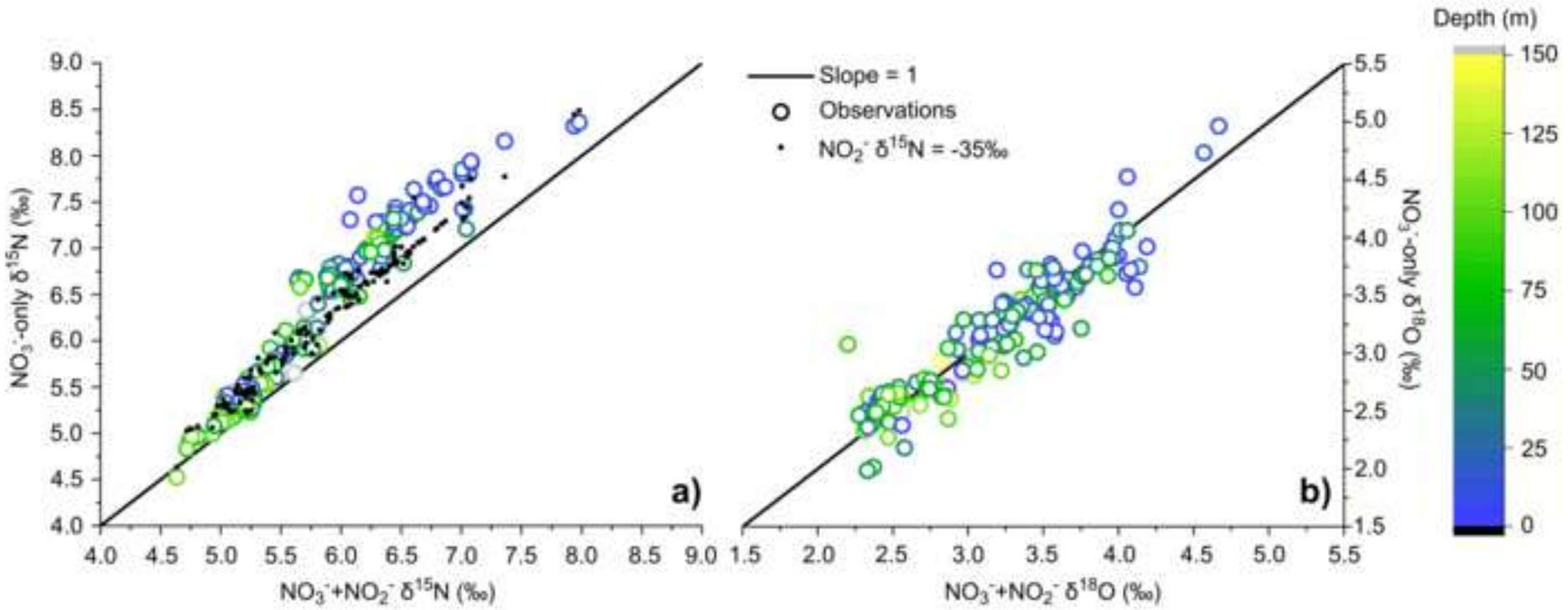

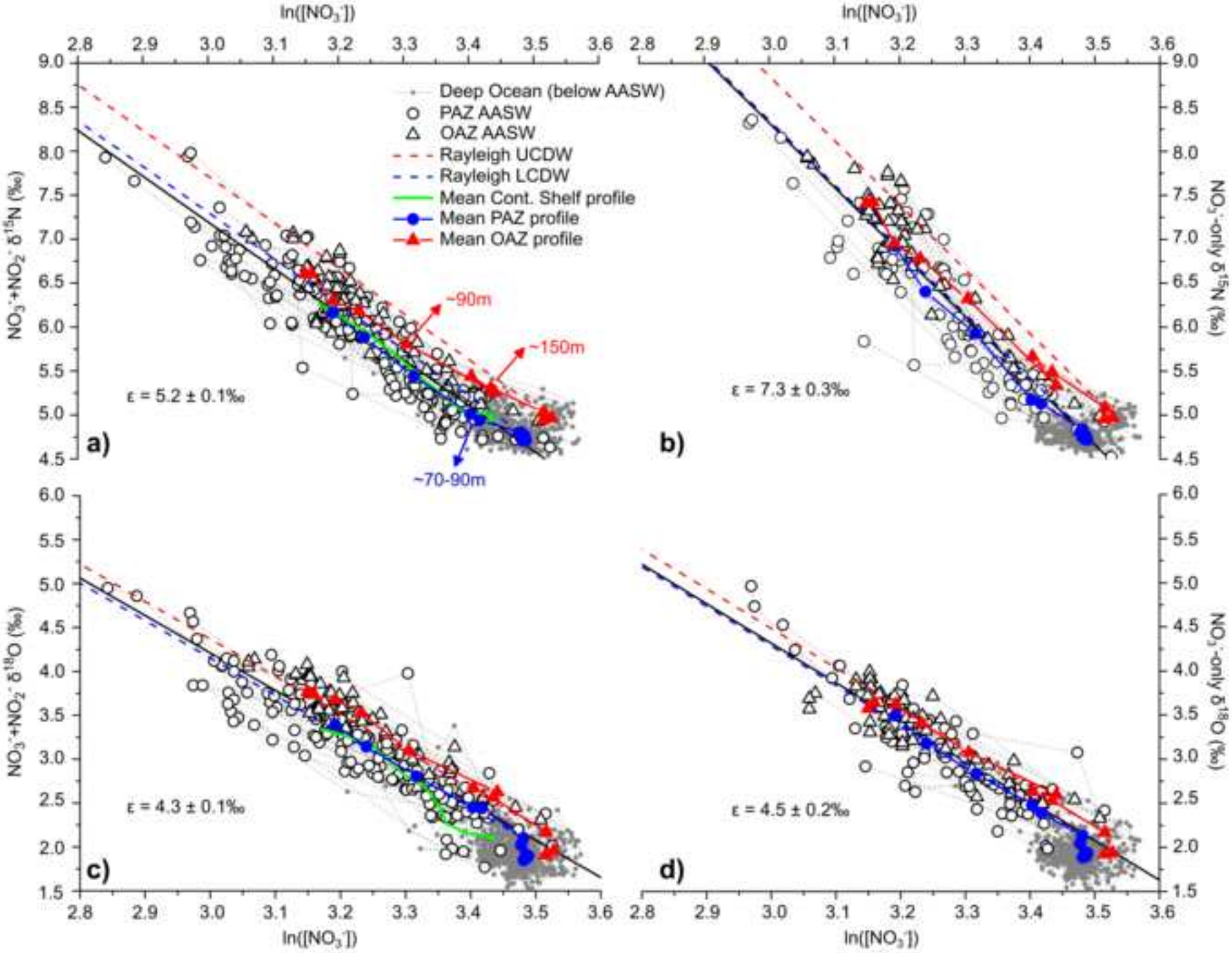

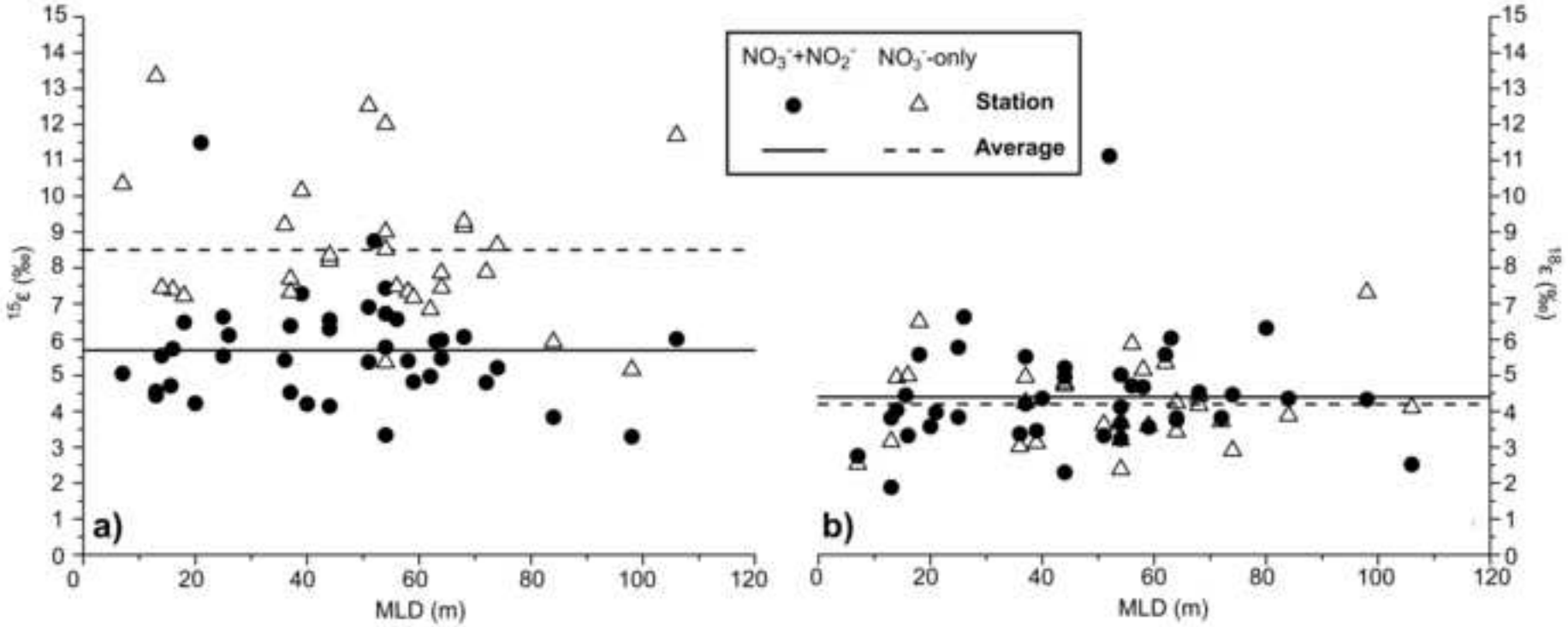

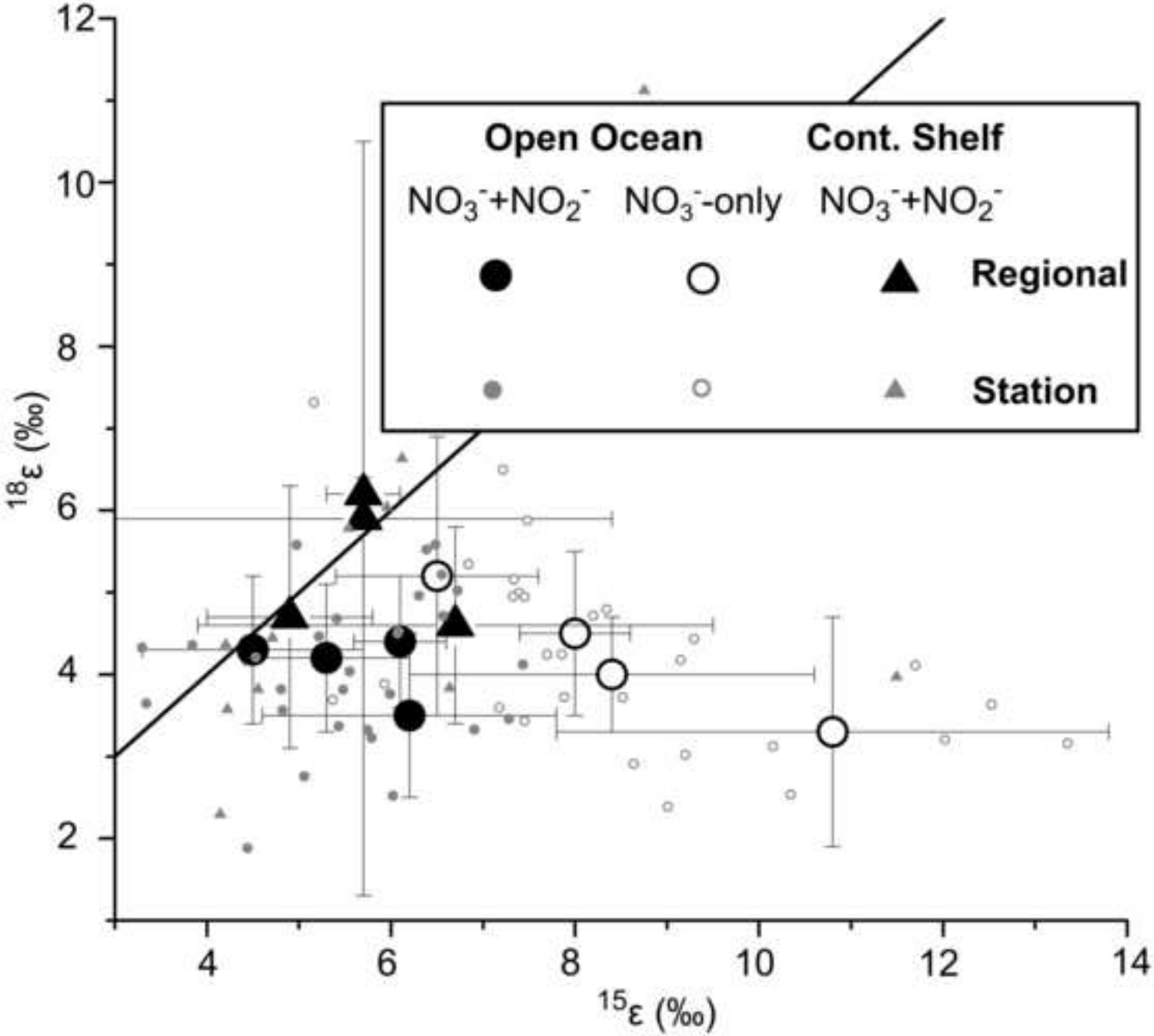

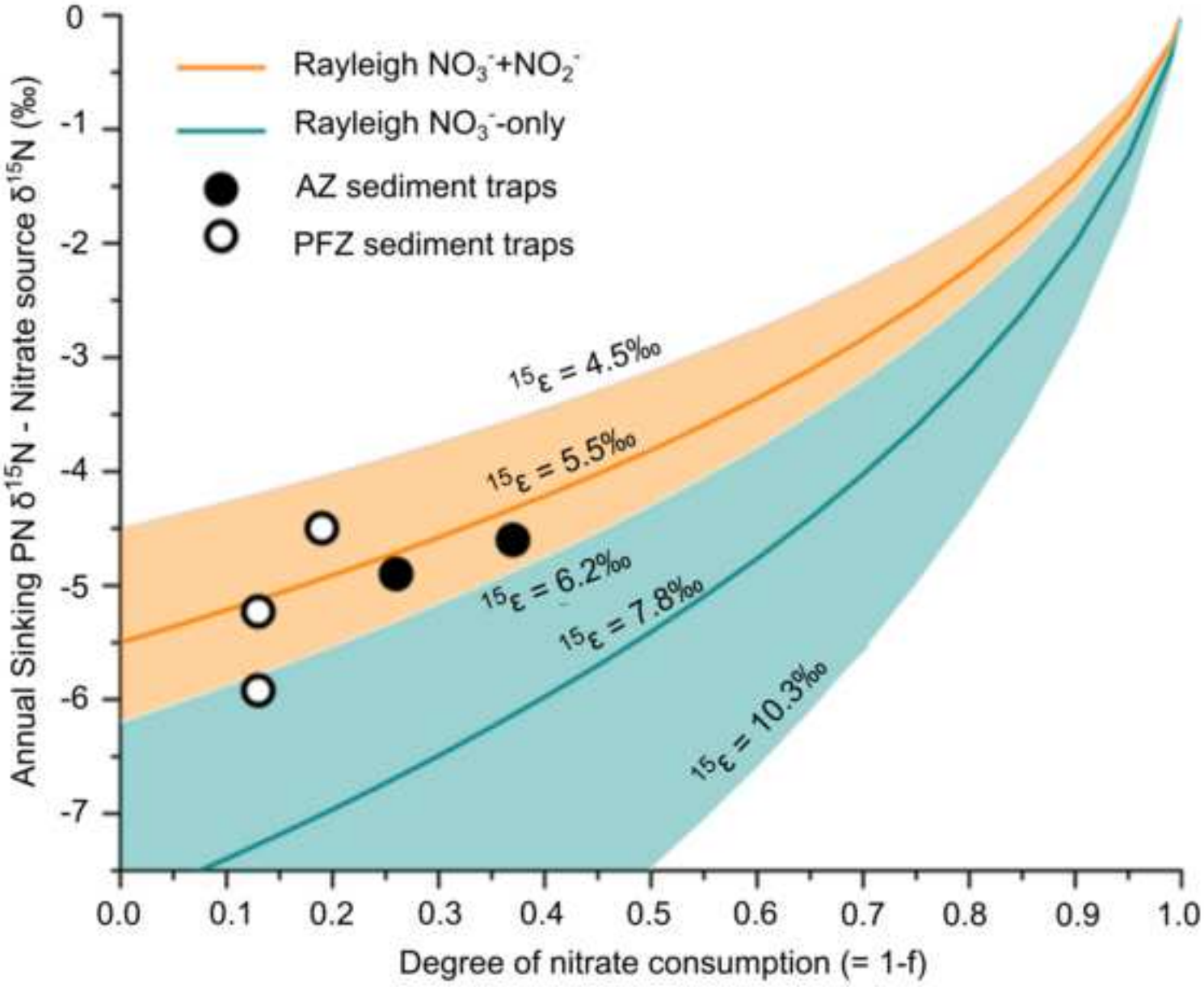

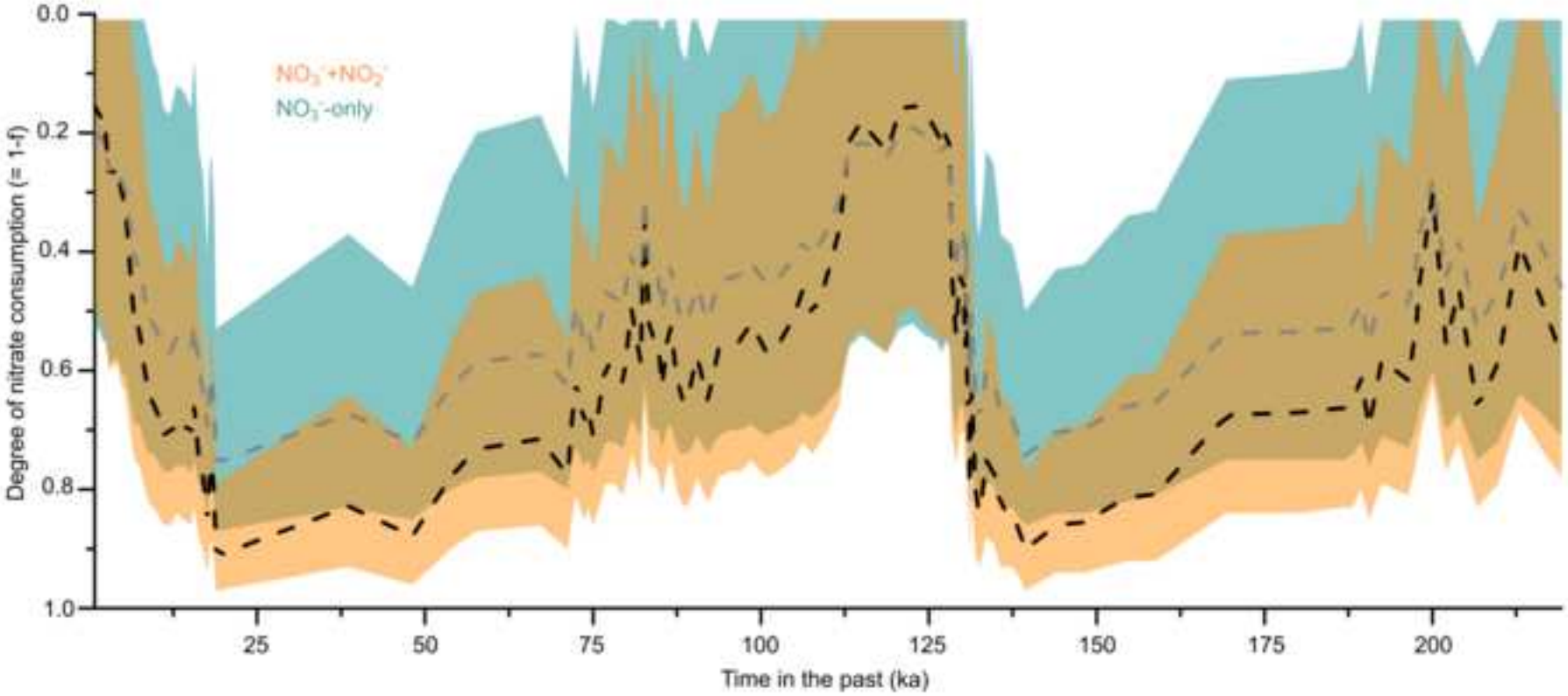

Cruise (Sector)	Name	Location	Date	PAZ #	OAZ #	Regional ε average (‰) $NO_3^-+NO_2^-$ $^{15}\varepsilon$	Regional ε average (‰) $NO_3^-+NO_2^-$ $^{18}\varepsilon$	Regional ε average (‰) NO_3^--only $^{15}\varepsilon$	Regional ε average (‰) NO_3^--only $^{18}\varepsilon$	Station ε average[5] (‰) $NO_3^-+NO_2^-$ $^{15}\varepsilon$	Station ε average[5] (‰) $NO_3^-+NO_2^-$ $^{18}\varepsilon$	Station ε average[5] (‰) NO_3^--only $^{15}\varepsilon$	Station ε average[5] (‰) NO_3^--only $^{18}\varepsilon$
IO8 (Indian)		83°E	Feb. 2016	6	3	5.9± 0.4	4.4± 0.3	7.6± 0.6	4.2± 0.3	6.1± 0.5	4.3± 0.8	8.0± 0.6	4.5± 1.0
P16 (Pacific)[1]		150° W	Apr. 2014	6	2	4.9± 0.3	4.6± 0.3	6.7± 0.5	4.5± 0.3	5.3± 0.9	4.2± 0.9	8.4± 2.2	4.0± 0.7
P18 (Pacific)		103° W	Jan. 2017	2	5	5.8± 0.5	4.8± 0.5	8.4± 0.7	4.2± 0.5	6.1± 1.6	3.5± 1.0	10.8± 3.0	3.3± 1.4
SANAE54 (Atlantic)		0°W	Dec-Feb 2014-2015	7	1	4.8± 0.3	4.3± 0.2	6.2± 0.2	4.8± 0.3	4.5± 1.3	4.3± 0.8	6.4± 1.1	5.2± 1.7
NBP01-01 (DDU[2])[3]		146°E	Feb. 2001	6	0	3.2± 0.4[4]	1.9± 0.9[4]			5.7± 2.7	5.9± 4.6		
NBP01-01 (Davis Sea)[3]		93°E	Feb. 2001	3	0	4.9± 0.4	4.8± 0.8			4.9± 0.9	4.7± 1.6		
NBP01-01 (Prydz Bay)[3]		76°E	Mar. 2001	5	0	3.8± 0.6[4]	4.2± 0.7[4]			6.7± 2.8	4.5± 1.2		
NBP06-08 (Ross Sea)[3]		174°E	Nov. 2006	4	0	5.8± 0.5	6.3± 0.8			5.7± 0.4	6.2± 0.2		
AASW average				**39**	**11**	**5.2± 0.1**	**4.2± 0.1**	**7.3± 0.3**	**4.5± 0.2**	**5.7± 1.5**	**4.4± 1.5**	**8.5± 2.0**	**4.2± 1.1**
AASW average (without DDU and Ross Sea)[4]				**29**	**11**	**5.4± 0.2**	**4.6± 0.1**						

[1]Kemeny et al., 2016

[2]Dumont D'Urville Sea

[3]DiFiore et al., 2009

[4]The variability in the AASW for these areas is close to the analytical precision

[5]Only the stations with a vertical isotopic gradient greater than 0.2‰ are used

WW conditions	ML conditions	$NO_3^-+NO_2^-$ $^{15}\varepsilon$ (‰)	NO_3^--only $^{15}\varepsilon$ (‰)
PAZ	PAZ	5.4	10.4
OAZ	OAZ	5.4	8.0
PAZ	OAZ	6.8	12.6
OAZ	PAZ	4.3	5.9
Mixture PAZ-OAZ	PAZ	4.8	7.8
Mixture PAZ-OAZ	OAZ	6.7	11.1
	Average	5.6	9.3
	sd	1.0	2.5

	NO_3^-+NO_2^-	NO_3^--only
N isotope effect[a]	4.5-6.7‰	6.2-10.8‰
Source NO_3^- $\delta^{15}N$[b]	5.0-6.2‰	5.1-6.0‰
Source NO_3^- concentration[b]	24-32 µmol l^{-1}	24-32 µmol l^{-1}
Summer surface NO_3^- concentration[c]	~24 µmol l^{-1}	~24 µmol l^{-1}
Modern surface NO_3^- consumption[d]	~20%	~20%
Core-top diatom-bound $\delta^{15}N$[e]	2.2‰	2.2‰
Expected sinking PN $\delta^{15}N$[f]	0.4‰	-2.1‰
Isotopic offset[g]	1.8‰	4.3‰
LGM diatom-bound $\delta^{15}N$[e]	6.2‰	6.2‰
LGM Expected sinking PN $\delta^{15}N$[h]	4.4‰	1.9‰
LGM surface NO_3^- consumption	79-97%	53-87%
LGM summer surface NO_3^- concentration	0.7-6.7 µmol l^{-1}	3.1-15.4 µmol l^{-1}

[a]Range given by the regional and station $^{15}\varepsilon$ averages (Table 1)

[b]Range given by the Tmin average for each individual cruises

[c]Average for the Antarctic Zone summer mixed layer

[d]Based on the average for the Antarctic Zone T_{min} and summer mixed layer

[e]Based on Studer et al. (2015)

[f]Estimated based on the AASW Rayleigh fractionation trends

[g]Difference between core-top diatom-bound and expected sinking PN $\delta^{15}N$

[h]LGM diatom-bound $\delta^{15}N$ minus the isotopic offset

	$NO_3^-+NO_2^-$ $^{15}\varepsilon$ (‰)	NO_3^--only $^{15}\varepsilon$ (‰)	Study
Nutrient-replete regions			
Antarctic Zone	4.5-6.1	6.7-10.8	This study
Subantarctic Zone		8.0-9.0[1]	DiFiore et al., 2006
Subarctic Pacific	4.7-5.5		Brunelle, 2009
Subarctic Pacific		5.8-6.9	Wu et al., 1997
Subarctic Pacific		9.1[1]	Altabet and Francois, 1994
Equatorial Pacific	5.2	3.2-6.7	Altabet, 2001; Rafter and Sigman, 2016
California Current		4.9-5.2[1]	Altabet et al., 1999
Subarctic North Atlantic	5.2-5.3	5.1-5.2	Peng et al., 2018
Nutrient-depleted regions			
Sargasso Sea	-1.2 – 2.4	2.2-5.0	Fawcett et al., 2015
Eastern North Atlantic	2.7	3.5	Peng et al., 2018

[1]Acidified samples only